Tbx1 ortholog *org-1* is required to establish testis stem cell niche identity in *Drosophila*

Patrick Hofe[1], Ariel Harrington[1], Tynan Gardner[2], Stephen DiNardo[2], Lauren Anllo[1]*

[1] Department of Biology, East Carolina University, Greenville, NC 27858

[2] Perelman School of Medicine at the University of Pennsylvania, Philadelphia, PA 19104

*Communicating author: anllol22@ecu.edu

Abstract:

Stem cells require signals from a cellular microenvironment known as the niche that regulates identity, location, and division of stem cells. Niche cell identity must be properly specified during development to form a tissue capable of functioning in the adult. Here, we show that the Tbx1 ortholog *org1* is expressed in *Drosophila* testis niche cells in response to Slit and FGF signals. *org1* is expressed during niche development and is required to specify niche cell identity. *org1* mutants specified fewer niche cells, and those cells showed disruption of niche-specific markers, including loss of the niche adhesion protein Fas3 and reduced *hedgehog* expression. We found that *org1* expression in somatic gonadal precursors is capable of inducing formation of additional niche cells. Disrupted niche identity in *org1* mutants resulted in niche assembly and functionality defects. We find the conserved transcription factor *islet* is expressed in response to *org1* and show that *islet* functions downstream to mediate niche identity and assembly. This work identifies a novel role for *org1* in niche establishment.

Summary Statement:

Specification of niche identity is crucial to establish a functional stem cell microenvironment. Using a translatable model, we show that niche expression of *org1* influences *islet* to specify niche identity.

Introduction:

Stem cells play a vital role in maintaining functional tissues. The preservation of stem cells in many tissues is controlled by the stem cell niche, a local cellular microenvironment that supplies signals to maintain stem cell identity, location, and division rates (Li & Xie, 2005). A key concept in stem cell biology is use of diffusible signals to regulate stem cell behaviors. In models like the mammalian intestinal stem cell (ISC) niche, diffusible signals such as Wnt, Hh, and BMP regulate stem cells (Walker et al., 2008). These signals have varying origins since there are multiple cell types that comprise the intestinal stem cell niche (Walker et al., 2008). Because various cell lineages can comprise the niche, identification of niche cells is often challenging. In some tissues even the identity of the stem cells is unclear (Sato et al., 2011; Kaestner, 2019; Li et al., 2023). Thus, identifying regulators that specify niche identity during tissue development has remained a challenge in stem cell biology.

Because of its readily identifiable, well-defined niche, we leverage the *Drosophila* testis to study how niche cells acquire their identity and adopt proper function during development (de Cuevas & Matunis, 2011;Le Bras & Van Doren, 2006;Anllo et al., 2019;Okegbe & DiNardo, 2011;Wingert & DiNardo, 2015). The *Drosophila* testis is a paradigmatic niche in which many concepts at the foundation of stem cell biology continue to be elucidated (Herrera & Bach, 2019; Leatherman & DiNardo 2008 and 2010; Lenhart & DiNardo 2015; Inaba et al., 2015; Tulina & Matunis 2001; Yamashita et al., 2003; Zheng et. al., 2011). The singular cell type that comprises the testis niche, somatic “hub” cells, regulates germline and somatic stem cells required to maintain sperm production throughout the adult life of the fly (Lenhart and DiNardo, 2015; Roach and Lenhart, 2024). The wealth of powerful genetic tools available to study this niche make it an ideal model to identify regulators of niche cell fate.

Prior to niche formation, the embryonic Stage 15 *Drosophila* testis is a spherical arrangement of somatic gonadal precursors (SGPs) interspersed among and encysting germ cells (Jenkins et al., 2003; Le Bras & Van Doren, 2006). SGPs are specified from a subset of mesodermal cells adjacent to muscle precursors in embryonic parasegments 10-13 earlier in embryogenesis (Boyle et al., 1995; Boyle et al., 1997; Riechmann et al., 1998). Niche, or “hub,” cells derive from SGPs, and are initially specified through Notch signaling (Kitadate & Kobayashi, 2010; Okegbe & DiNardo, 2011; DiNardo et al., 2011). By stage 11 of embryogenesis, SGPs contacting the primordial midgut receive Delta ligands which initiate Notch signaling and niche specification (Okegbe & DiNardo, 2011). Continued specification, or further induction of niche cell identity after the initial acquisition of niche cell fate, is required to establish the niche. As part of continued specification, SGPs at the gonad anterior receive the

56 Notch ligand Serrate from other gonadal cells, and SGPs at the posterior receive EGFR
57 antagonistic signals that repress niche identity (Kitadate & Kobayashi, 2010). Defects in Notch
58 signaling result in fewer niche cells specified (Okegbe & DiNardo, 2011; DiNardo et al., 2011;
59 Kitadate & Kobayashi, 2010; Wingert & DiNardo, 2015). Specified niche cells downregulate the
60 conserved Maf transcription factor Traffic jam (Tj) in response to Notch (Wingert & DiNardo,
61 2015). A role for Notch signaling in niche formation has translated to other niches in *Drosophila*
62 and in mammals (Zamfirescu et al., 2022). Outside of Notch signaling, there is little known about
63 how testis niche cells acquire their identity.
64 After the initiation of specification, embryonic niche cells are compartmentalized to the
65 gonad anterior in a process called niche assembly (Le Bras & Van Doren, 2006; Anllo et al.,
66 2019). During assembly, specified prospective (pro) niche SGPs move peripherally onto the
67 gonadal extracellular matrix (ECM), where they then migrate to their anterior assembly position
68 (Anllo et al., 2019). Our previous work revealed that extrinsic Slit and FGF signals from
69 neighboring visceral muscle (Vm) are required for this migration (Anllo & DiNardo, 2022). At the
70 gonad anterior, niche cells first exhibit F-actin polarization to niche-niche interfaces, which later
71 re-polarizes to niche-stem cell interfaces as niche cells compact into a spherical arrangement
72 with smooth contour (Anllo & DiNardo, 2022; Warder et al., 2024). Germline stem cells
73 contacting the assembled niche contribute to niche morphogenesis through actomyosin
74 networks that result in tension around the compacting hub periphery (Warder et al., 2024). The
75 assembled and compacted niche expresses niche specific markers such as *fasciclin3* and
76 *hedgehog* and is radially surrounded by germline stem cells (GSCs) and later, cyst stem cells
77 (CySCs) (Le Bras & Van Doren, 2006; Sheng et al., 2009; Sinden et al., 2012; Wingert &
78 DiNardo, 2015). The niche makes adhesive connection to neighboring stem cells and
79 extracellular matrix to maintain its shape, location, and function (Lee et al., 2008; Vida et al.,
80 2024; Tanentzapf et al., 2007; Tseng et al., 2022; Amoyel et al., 2013).
81 After niche establishment, the niche functions throughout the life of the animal. The
82 niche's location, critical to maintain GSCs and CySCs, is maintained through Integrin-mediated
83 connections to the ECM (Anllo et al. 2019; Lee et al., 2008; Tanentzapf et al., 2007). In its
84 established position, the niche sends maintenance signals to its surrounding stem cells,
85 including Unpaired (Upd) and Hedgehog (Hh). Upd ligands activate JAK/STAT signaling in
86 GSCs, which regulates their adhesion to the niche and oriented cell divisions (Chen et. al.,
87 2018; Leatherman & DiNardo 2008 and 2010; Tulina & Matunis, 2001; Wawersik et al., 2005;
88 Yamashita et al., 2003). Niche-secreted Hedgehog regulates CySC self-renewal (Amoyel et al.,

2012). Niche signals are important for establishing the stem cell populations, and for long term stem cell maintenance (Sheng et al., 2009; Sinden et al., 2012).

Because Notch signaling required to specify niche cells is initiated at stage 11 of embryogenesis (Okegbe & DiNardo, 2011), and niche-specific markers such as Fas3 accumulation are not observed until stage 15 of embryogenesis (Le Bras & Van Doren, 2006; Anllo et al., 2019), there are likely other factors influencing the specification of niche cells during this period. Our work here identifies the Tbx1 ortholog *org1* as one of those factors. Tbx1 and its orthologs play a conserved role across phyla in specifying mesodermal cell types (Marcellini et al., 2003). Like Tbx1*, org1* encodes a transcription factor with a T-box DNA binding domain and is a known regulator of mesodermal muscle fate during embryonic development (Schaub et al. 2012; Schaub & Frasch, 2013; Boukhatmi et al., 2014). Our previous work identified that the conserved transcription factor *islet* is expressed in niche cells and required for both niche assembly and cytoskeletal polarization downstream of Vm assembly cues (Anllo & DiNardo, 2022). *islet* expression is known to be regulated by *org1* during specification of alary musculature (Boukhatmi et al., 2014). Here, we find that a parallel mechanism regulates continued specification of niche cells and directs their anterior assembly. We show that *org1* is expressed in the embryonic niche and reveal its requirement in establishing a full complement of functional, assembled niche cells. We further show that Org1 accumulation is affected by Slit and FGF signals, and that *islet* acts downstream of *org1*. These data reveal *org1* as a novel regulator of niche identity and assembly for the *Drosophila* testis niche.

Results:

org1 is expressed in the niche and is induced by Slit and FGF signals.

Our previous work has shown that the conserved transcription factor *islet* is expressed in the developing niche (Anllo & DiNardo, 2022). Because Org1 is a known regulator of *islet* in other tissues (Boukhatmi et al., 2014), and single nuclear RNA sequence data (snRNAseq) suggested that *org1* was enriched in the adult testis niche (Li et al., 2021; Raz et al. 2023), we tested whether *org1* was expressed in the developing gonadal niche. Using an Org1::GFP transgenic BAC reporter that rescues *org1* lethality (Kudron et al., 2018 and data not shown), we observed Org1 in prospective niche cells beginning prior to assembly at embryonic stage 15/16 and after niche assembly in stage 17 at the gonad anterior (Figure 1A-1C'). Org1::GFP detection in some

122 prospective niche cells coincided with the timing of Traffic jam downregulation (Figure 1A', 1B').
123 Additionally, we also saw SGPs without downregulated Traffic jam that exhibited lower levels of
124 Org1::GFP elsewhere in the gonad (Figure 1B-B", yellow arrows). We confirmed the stage 17
125 Org1::GFP expression pattern using an Org1 antibody (Schaub et al., 2012) that revealed a
126 signal in gonadal niche cell nuclei (Figure 1D, D') which was absent in *org1* mutants (Figure
127 S1). Our findings reveal that *org1* is expressed in the gonad niche, and its expression begins
128 before niche assembly.
129
130 Since *islet* is regulated by Slit and FGF signals from the visceral muscle (Vm), we tested if *org1*
131 is also regulated by these signals (Anllo and DiNardo, 2022). If *org1* is induced by these signals,
132 then loss of Slit and FGF Vm signals required for niche assembly would result in loss of Org1
133 accumulation in niche cells. We assessed Org1 accumulation in double mutant animals with the
134 *slit[2]* mutation and the small chromosomal deficiency Df(2R)BSC25 that removes both genes
135 encoding FGF Heartless ligands, *pyramis* and *thisbe* (see Methods). Indeed, loss of both
136 signals together resulted in diminished Org1 accumulation (Figure 1E-1F'). Additionally, loss of
137 either Slit or FGF separately resulted in diminished Org1 accumulation (Figure 1G-1H') and our
138 fluorescence quantifications supported these findings (Figure 1I-1K). Together, our data confirm
139 that *org1* is expressed in the niche and accumulates in response to Slit and FGF.

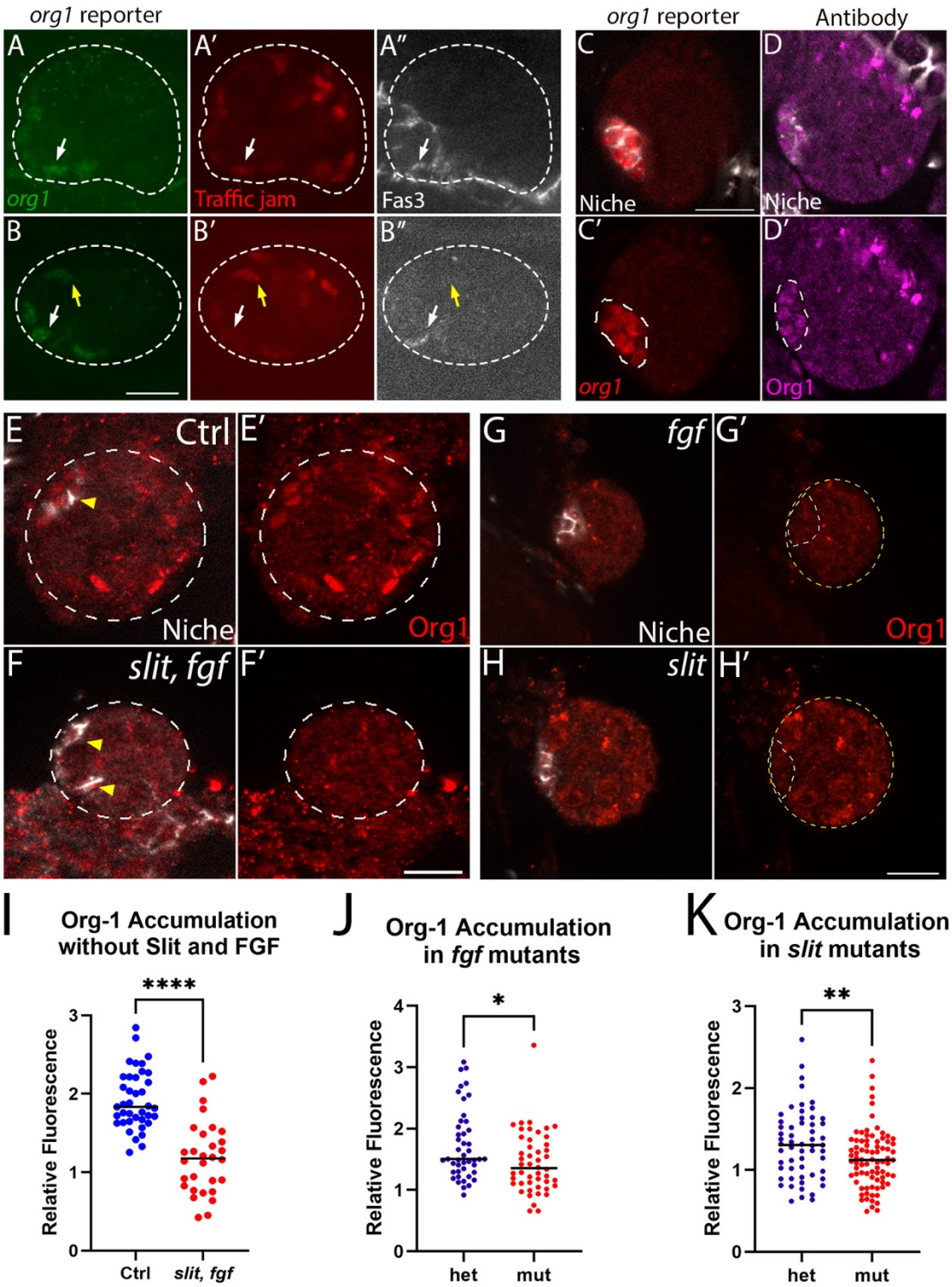

Figure 1. *org1* is expressed in the niche in response to Slit and FGF signals. (A-B') Gonads (dotted line) from Stage 15 animals with the Org1::GFP BAC reporter, immunostained for GFP (green) and Traffic jam (red). Fas3 (white) accumulates at assembling niche cell interfaces. Org1::GFP is brightest when Traffic jam (red) is downregulated. Prospective niche cells with downregulated Traffic jam (white arrows) and with Traffic jam not downregulated

146 (yellow arrows). (C-H) Gonads dissected from Stage 17 animals aged 20-22 hours at 25
147 degrees C. (C, C') Org1::GFP reporter (red) showed *org1* expression in the assembled niche
148 (dotted white line; Fas3, white). (D, D') Org1 antibody (magenta) revealed accumulation in the
149 niche (dotted white line; Fas3, white) with spurious non-specific signal at the posterior (see
150 Suppl Fig S1). (E-H) Dissected Stage 17 gonads immunostained to reveal Org1 (red) and the
151 Niche (Fas3, white). (E, E') Control gonads showed Org1 (red) accumulation in the niche
152 (white). (F, F') *slit, fgf* mutants had diminished accumulation of Org1. Gonads are outlined with
153 dotted lines. (G-G') *fgf* mutants had diminished niche Org1 accumulation. (H, H') *slit* mutants
154 had diminished niche Org1 accumulation. Gonads are outlined in yellow; niches are outlined in
155 white. (I) Quantification of Org-1 accumulation in niche cells in controls and Slit and FGF
156 signaling mutants ($p<0.0001$, Ctrl n=39 niche cells from 13 gonads; *slit, fgf* n= 30 niche cells,
157 from 10 gonads Mann-Whitney Test). (J) Quantified Org1 accumulation in *fgf* mutants and
158 heterozygous sibling controls (Het) ($p= 0.0136$, Het n=45 niche cells from 15 gonads; *fgf* n=48
159 niche cells from 16 gonads, Mann-Whitney Test). (K) Quantified Org1 accumulation in *slit*
160 mutants and heterozygous sibling controls (Het) ($p= 0.0090$, Het n=57 niche cells from 19
161 gonads; *slit* n=81 niche cells from 27 gonads, Mann-Whitney Test). All quantifications are
162 shown for individual niche nuclei. Scale bars, 10um. $n\geq3$ trials.
163

164 ***org1* is necessary and sufficient for aspects of niche cell identity.**

165 Given the known role of *org1* in embryonic muscle specification, we asked if there were niche
166 identity defects in *org1* mutants (Schaub & Frasch, 2012; Boukhatmi et al., 2014). We
167 hypothesized that if *org1* had a role in specifying niche fate, we would see disruption of identity
168 markers. We assayed for niche identity markers Fasciclin3 (Fas3) accumulation and *hedgehog*
169 (*hh*) expression (Le Bras & Van Doren, 2006; Wingert & DiNardo, 2015) in an *org1* mutant allele
170 lacking the translation initiation codon and T-box domain (Schaub et al., 2012). *org1* mutants did
171 not accumulate the niche specific adhesion protein Fasciclin 3 (Figure 2B-2B'). Additionally,
172 *org1* mutants had lower expression of a *hh*-lacZ reporter in niche cells compared to controls
173 (Figure 2C-2E). Interestingly, *hh* expression is known to be restricted to the adult niche (Amoyel
174 et. al., 2013). We find that while *hh* expression is highest in control embryonic niche cells, we
175 detect low levels of *hh* in some control SGPs outside the niche (Figure S2). Since these niche
176 identity markers were disrupted, we used N-cadherin (N-cad) accumulation to detect niche cells
177 in *org1* mutants. N-cad accumulation is enriched at the cortex of properly assembled anterior
178 niche cells, with low accumulation in other SGPs, affording a reasonable measure of
179 identification of niche cells at the anterior (Le Bras & Van Doren, 2006). When visualizing
180 gonads with N-cad immunofluorescence, we detected fewer N-cad accumulating niche cells in
181 *org1* mutants compared to controls (Figure 2F-2G'). The detection of N-cad in some cells
182 indicates that not all aspects of niche identity are disrupted, suggesting a role for *org1* in
183 continued induction of niche fate after their initial specification.
184

To confirm that the fewer N-cad accumulating niche cells in *org1* mutants resulted from failure of continued niche cell specification in *org1* mutants, and not simply a reduction in the number of SGPs, we quantified the total number of SGPs in *org1* mutants. We assayed the SGP-specific transcription factor Traffic jam (Tj) to count all SGPs (Wingert & DiNardo, 2015). While there was a slight decrease in number of SGPs, the fraction of these cells specified into niche cells was significantly lower in *org1* mutants compared to control gonads (Figure S3). Together with our data indicating a loss of the niche specific adhesion protein Fas3 and reduction of *hh* gene expression in the niche, these results support a role for *org1* in continued specification of niche identity (Figure 2, S3). Interestingly, *org1* mutant niche cells still down regulated *tj* as in normal niches, indicating that some aspects of niche specification occur (Figure S3).

Since *org1* mutants had fewer niche cells, we tested whether overexpression of *org1* in all SGPs would create more niche cells. Indeed, when overexpressing *org1* with a somatic lineage-specific driver (*six4*-gal4; Anllo et. al., 2019), we generated additional N-cad and Islet accumulating niche cells at the gonad anterior (Figure 2I-K; 5E-F). Together, our data suggest that *org1* plays a role in specifying niche identity and is sufficient to induce niche identity in additional SGPs.

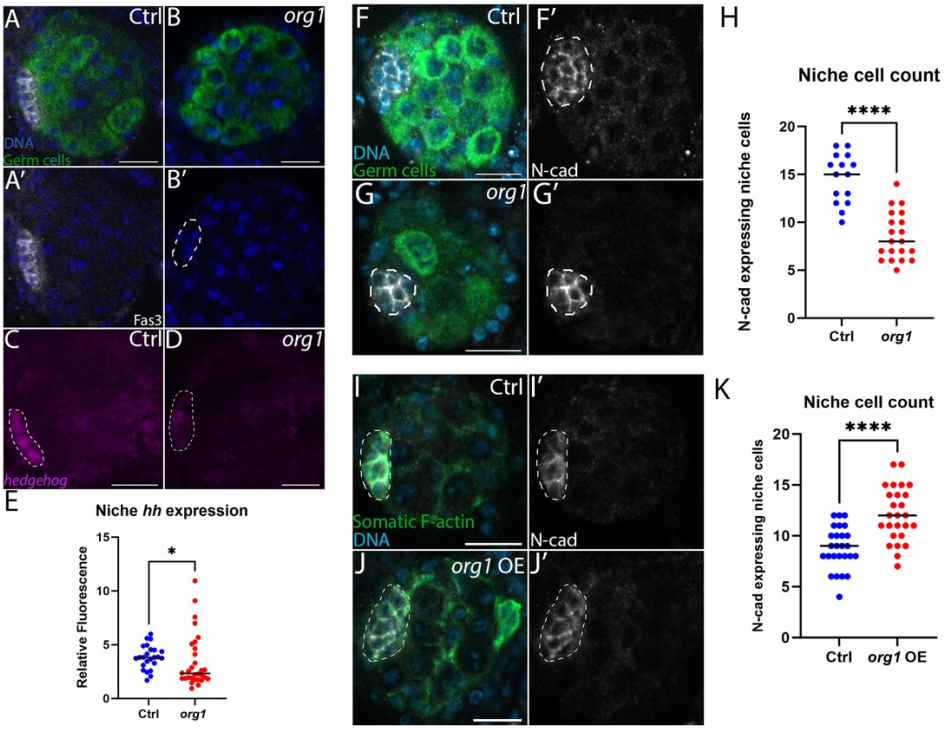

Figure 2. *org1* is necessary and sufficient for aspects of niche cell identity. (A-D) Dissected gonads immunostained to show germ cells (green), Fas3 (white), *hh*-lacZ (magenta),

DNA (blue). (A, A', C) Control niche cells accumulated niche specific markers Fas3 and *hedgehog* reporter expression (*hh*-lacZ, separate gonad from A, A'). (B, B', D) *org1* mutants did not accumulate Fas3 and had diminished expression of *hh*-lacZ (D is a separate gonad from B). (E) Quantified *hh*-lacZ expression in niche cells accumulating N-cad (p= 0.0294, Ctrl n=24 niche cells from 7 gonads; *org1* n=30 niche cells from 10 gonads, Mann-Whitney Test). (F, F') Control gonads accumulated enriched N-cad at the cortex of niche cells. (G, G') *org1* mutant niches had fewer cells accumulating enriched N-cad. (F-G') Germ cells (green), N-cad (white), DNA (blue). (H) Quantification of N-cad accumulating niche cells per gonad (p<0.0001, Ctrl n=15 gonads; *org1* n=20 gonads, Mann-Whitney Test). (I, I') Control gonad with *six4*moesinGFP marking somatic F-actin. (J, J') SGP driven *org1* overexpression in gonads generated niches that had more cells in comparison to controls. (I-J') Somatic cells (green), Niche (white), DNA (blue). (K) Quantification of niche cell count (p<0.0001, Ctrl n=26 gonads; *org1* n=26 gonads, Mann-Whitney Test). Dotted lines, niche. Scale bars, 10 um. n≥3 trials.

org1 is required SGP intrinsically for niche identity and assembly.

The data above were collected from a whole organism *org1* mutant line in which all T-box binding domains were excised (Schaub et al., 2012). To test whether *org1* is required autonomously in SGPs, we disrupted *org1* using two somatic lineage-specific drivers that varied in strength, *six4*VP16-gal4 (Warder et al., 2024) and *six4*-gal4. Using the weaker driver (*six4*-gal4), we found an expected decrease in niche cell number, and Fas3 accumulation appeared reduced (Figure S4). Assuming this driver generates only a partial knockdown, this suggests a stringent requirement of *org1* in niche cell specification (See Discussion). Excitingly, using the stronger driver (*six4*VP16-gal4), we saw both fewer niche cells (Figure 3A-3C), and dispersed niche cells accumulating low levels of Fas3 (Figure 3B'-3B'', 3D). It is possible this dispersed phenotype was not something we could observe in the global *org1* mutants due to the complete loss of Fas3 (Figure 2). Other niche cell markers, including E-cad and N-cad, accumulate on control non-niche SGPs to a degree, so dispersed niche cells might not have been apparent (Figure S5). Our data suggest that *org1* is primarily a specification factor during niche establishment and secondarily affects niche assembly.

To further support an SGP intrinsic requirement for *org1* during niche establishment, we performed a tissue-specific rescue experiment. We expressed *org1* with our somatic lineage specific driver, *six4*-gal4, in whole organism *org1* mutants and observed rescued Fas3 accumulation (Figure 3E-3H'). Our rescue experiment simultaneously expressed the F-actin label Ftractin-tdTomato in SGPs, allowing analysis of niche cytoskeletal polarity. Our previous work has shown that F-actin polarizes to niche-stem cell interfaces after assembly is complete (Anllo & DiNardo, 2022; Warder et al., 2024). While F-actin polarization at niche-stem cell interfaces is disrupted in *org1* mutant niche cells, this polarization was rescued with *org1* overexpression in SGPs (Fig 3F-K, see arrows). These data suggest that *org1* in SGPs is

244 sufficient to initiate downstream cell biological events that polarize F-actin in the assembled
245 niche.
246

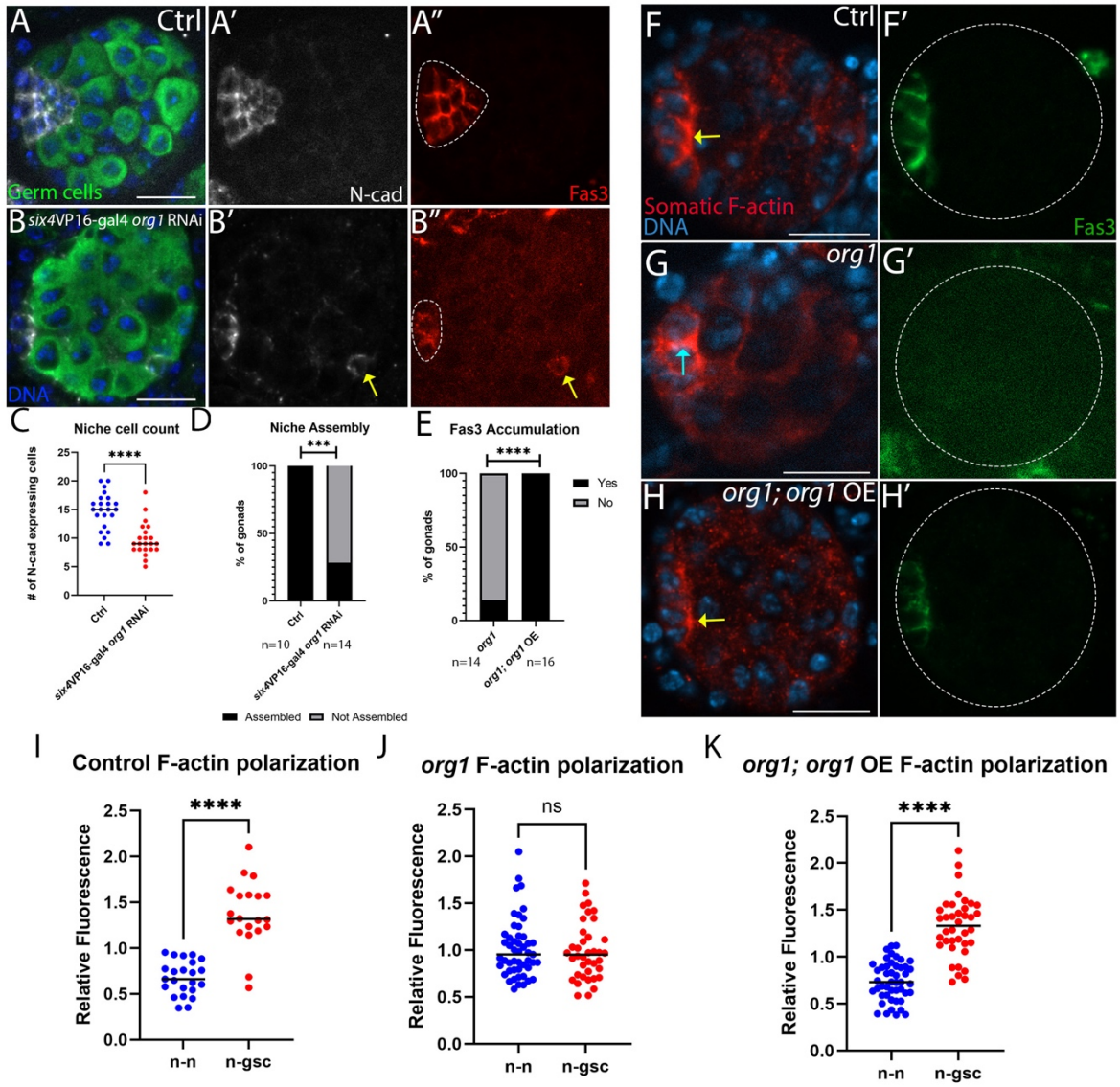

247

248 **Figure 3. *org1* is required SGP intrinsically for niche identity and assembly.** (A, A', A'')
249 Control gonads with N-cad (white) and Fas3 (red) accumulating at the anterior. (B, B', B'') *org1*
250 knockdown with six4gal4VP16 gonads showed fewer niche cells that accumulate N-cad (white)
251 and Fas3 (red) at the anterior, with displaced niche cells (yellow arrow). Brightness and contrast
252 were adjusted in A" and B" to enable visualization of Fas3. (C) Niche cell count per gonad in
253 *org1* knockdown ($p<0.0001$, Ctrl n=23 gonads; six4VP16-gal4 *org1* RNAi n=22 gonads, Mann-
254 Whitney Test). (D) Quantification of niche assembly in six4VP16-gal4 *org1* RNAi ($p= 0.0006$,
255 Ctrl n= 10 gonads; *org1* RNAi n=14 gonads, Fisher's Exact Test) (E) Quantified Fas3
256 accumulation in *org1* rescue niches ($p<0.0001$, *org1* n= 14 gonads; *org1; org1* OE n= 16
257 gonads, Fisher's Exact Test). (F-H) Yellow arrows indicate niche-GSC F-actin interfaces and
258 blue arrows indicate niche-niche F-actin interfaces. (F, F') Control gonad with Fas3 (green)

accumulating at the anterior. (G, G') *org1* knockout mutant gonad with no Fas3 (green) accumulation. (H, H') *org1* knockout mutant with *org1* overexpression in somatic gonadal cells (red) with rescued Fas3 (green) accumulation. (F-H) arrows indicate F-actin enrichment at specific SGP interfaces. (I) Quantified F-actin polarization in control gonads ($p<0.0001$, n-n interfaces n=23; n-gsc interfaces n=20, from 7 gonads, Mann-Whitney Test). (J) Quantified F-actin polarization in *org1* mutants (not significant, n-n interfaces n=49; n-gsc interfaces n=38, from 14 gonads, Mann-Whitney Test). (K) Quantified F-actin polarization in *org1* mutant rescued gonads ($p<0.0001$, n-n interfaces n=47; n-gsc interfaces n=38, from 16 gonads, Mann-Whitney Test). Scale bars, 10 um. $n\geq3$ trials.

org1 is important for niche to stem cell communication.

Given the defects in niche identity and organization seen when *org1* is compromised, we tested if the function was compromised without *org1*. We used known steady state niche signaling pathways and centrosome position to assay for niche function deficits (Leatherman & DiNardo, 2010; Kiger et al., 2001; Tulina & Matunis, 2001; Yamashita et al., 2003, 2005). Stat accumulates in GSCs in response to the niche signal Upd1 (Chen et al., 2018; Kiger et al., 2003). We assessed *upd1* expression in niche cells by quantifying levels of *upd1*-Gal4 driven RFP fluorescence and found significantly reduced expression in niche cells in whole organism *org1* mutants (Figure 4A-C). Additionally, we measured reduced Stat accumulation in GSCs (Figure 4D-4E', 4F), which was consistent with loss of *upd1* expression and impaired niche-GSC communication. Niche cells are also responsible for sending Hh signals to prospective CySCs to enable their self-renewal (Michel et al., 2012; Amoyel et al., 2013). We examined localization of Patched, a Hh receptor that accumulates in vesicles in the niche and CySCs in response to signaling (Amoyel et al., 2013; Michel et al., 2012; Wingert & DiNardo, 2015) (Fig 4G-4H'). *org1* mutants had significantly reduced Patched accumulation in the niche and never accumulated Patched in nearby somatic cells (Figure 4G-4H', 4I). This finding aligns with the reduced *hh* expression we detected in niche cells when *org1* was disrupted (Figure 2C-E), correlating reduced ligand expression to disruption in niche-CySC communication.

We also tested stem cell behavior in the absence of *org1*. During normal GSC divisions, one centrosome is anchored close to the niche-germline stem cell interface, while the other centrosome moves to the opposite GSC pole. The alignment of one centrosome at the niche interface enables GSC divisions perpendicular to the niche (Yamashita et al., 2003). Gonads from *org1* null animals showed defects in centrosome alignment, with both GSC centrosomes often displaced from the interface with the nearby niche cell. This displacement positioned centrosomes in orientations that would preclude perpendicular GSC divisions from the niche (Figure 4J-4K', 4L). Together, our data suggest that *org1* is required to generate niche cells

297 capable of communication with stem cells, further supporting a role for *org1* in niche cell
298 specification.
299
300 To ask whether *org1* is required cell autonomously in the somatic gonad to enable niche
301 communication with the stem cells, we assessed STAT and Patched accumulation in the
302 six4VP16-gal4 *org1* RNAi condition. Consistent with *org1* null animals, somatic gonadal
303 knockdown with *org1* RNAi resulted in failed accumulation of Patched in the niche and
304 neighboring somatic cells (Figure 4M-O), and failed accumulation of STAT in neighboring GSCs
305 (Figure 4P-R). These data indicate a cell autonomous requirement for *org1* in communication
306 with stem cells.
307
308 We hypothesized that failed communication to neighboring stem cells would adversely affect
309 stem cell maintenance. Neither *org1* null nor six4VP16-gal4 *org1* RNAi animals are viable past
310 embryogenesis, precluding analysis of later stem cell maintenance. We thus assessed GSC
311 maintenance by quantifying the number of STAT+ GSCs adherent to the embryonic niche. We
312 determined a threshold level of STAT+ accumulation quantified as one standard deviation below
313 the mean in control GSCs (see methods). Our data revealed significantly fewer STAT+ GSCs
314 (Figure 4S-T), and fewer total GSCs adherent to the niche (Figure 4U) in the six4VP16-gal4
315 *org1* RNAi somatic cell knockdown, which disrupts *org1* during niche specification and prior to
316 and through niche assembly. These data suggest functional defects in GSC maintenance when
317 *org1* is autonomously disrupted in the somatic gonad.
318

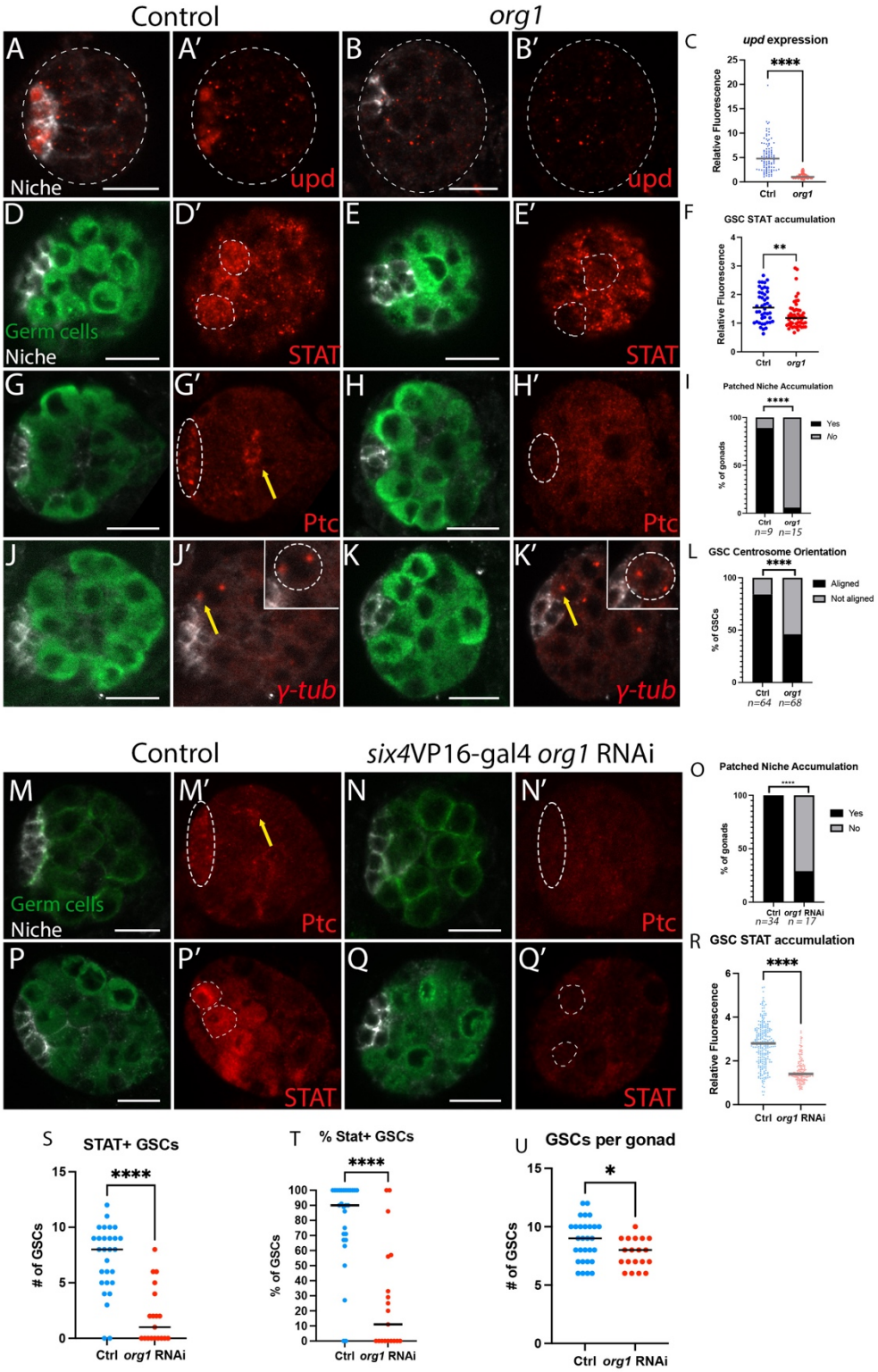

Figure 4. *org1* is important for niche to stem cell communication. (A, A') *upd1*-Gal4 drives RFP expression in control niche cells, but (B, B') not in *org1* null animals. (C) Quantification of RFP fluorescence in niche cells ($p < 0.0001$, Ctrl n = 100 niche cells from 20 gonads; *org1* n = 140 niche cells from 28 gonads) (D, D') STAT (red) accumulated in germline stem cells (GSCs,

dotted line) in control gonads, but (E, E') not in *org1* mutant germline stem cells. (F) Quantification of STAT accumulation (p= 0.0041, Ctrl n=44 GSCs from 11 gonads; *org1* n=52 GSCs from 16 gonads, Mann-Whitney Test). (G, G') Hedgehog signaling target Patched (red) accumulated in the niche (white dotted line) and Cyst stem cells (yellow arrow). (H, H'') Patched did not accumulate in *org1* mutant gonads in the niche or cyst stem cells. (I) Quantified Patched accumulation in the niche (p<0.0001, Ctrl n=9 gonads; *org1* n= 15 gonads, Mann-Whitney Test). (J, J') In control gonads with duplicated GSC centrosomes, one centrosome was aligned adjacent to the interface with the niche (yellow bracket). Insets show germline stem cells outlined in white, and the niche boundary (Fas3, white). (K, K') In *org1* mutant gonads, duplicated centrosomes were often not aligned adjacent to the niche interface (yellow bracket). (L) Quantified centrosome alignment (p<0.0001, Ctrl n=64 GSCs from 18 gonads; *org1* n= 68 GSCs from 21 gonads, Fisher's Exact Test). (J', K') Insets show centrosome pairs. (M-N) Hedgehog signaling target Patched accumulated in niche cells and CySCs in controls (M-M') but not in six4VP16-gal4 *org1* RNAi gonads (N-N'). (O) Quantified Patched accumulation in the niche (p<0.0001, Ctrl n=34 gonads; *org1* RNAi n= 17 gonads, Mann-Whitney Test). (P, P') STAT (red) accumulated in GSCs (dotted line) in control gonads, but (Q, Q') not in six4VP16-gal4 *org1* RNAi germline stem cells. (R-T) Quantified STAT accumulation (R), STAT+ GSCs (S), and percentage of GSCs that are STAT+ (T) (p<0.0001, Ctrl n=246 GSCs from 28 gonads; *org1* RNAi n=146 GSCs from 19 gonads, Mann-Whitney Test). (U) Number of GSCs contacting N-cad positive niche cells in control and six4VP16-gal4 *org1* RNAi gonads (p = 0.033, Ctrl n = 29 gonads, six4VP16-gal4 *org1* RNAi n = 19 gonads). For all panels: N-cad (white), scale bars, 10 um. Germ cells are indicated with *nos*-lifeactin::tdTomato (green, panels M-N) or Vasa (green, all other panels). n≥3 trials.

islet* regulates niche cell specification downstream of *org1

Our previous work has shown that *islet* is expressed downstream of Vm signals Slit and FGF and is important for niche assembly (Anllo & DiNardo, 2022). Here, we show *org1* is also expressed downstream of Slit and FGF and has a role in niche assembly (see Figure 1,3). Because *org1* is known to induce *islet* expression in embryonic muscle (Boukhatmi et al., 2014), we next tested if *org1* regulated *islet* in the embryonic gonad. Indeed, we saw that Islet was no longer enriched in *org1* mutant niche cells (Figure 5A-5C). We also hypothesized that if *org1* is regulating *islet*, we would see Islet accumulation in the additional niche cells specified with our SGP lineage specific *org1* overexpression. Indeed, we saw that additional niche cells at the anterior also accumulated Islet (Figure 5D-5F). These data indicate that Islet accumulates in response to *org1* expression.

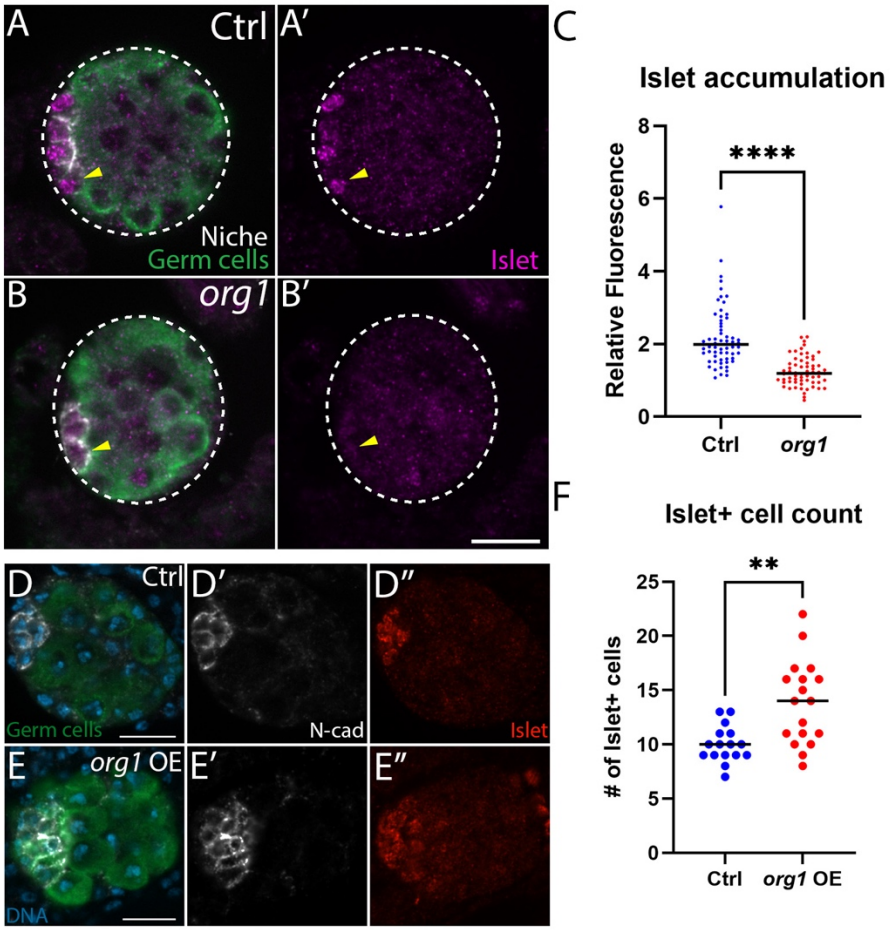

Figure 5. *org1* is important for Islet accumulation. (A, B) Germ cells (Vasa, green), Niche (Ncad, white), DNA (Hoechst, blue). (A, A') Control gonads showed Islet (magenta) accumulation enriched in the niche. (B, B') *org1* mutant gonads exhibited diminished Islet accumulation. (C) Islet accumulation quantification in niche cells ($p<0.0001$, Ctrl n=63 from 21 gonads; *org1* n=63 from 21 gonads, Mann-Whitney Test). (D, D', D'') Control gonads with N-cad (white) and Islet (red) accumulating in niche cells. (E, E', E'') *org1* overexpressing gonad with additional niche cells (white) that also accumulated Islet (red). (F) Quantification of number of Islet accumulating cells ($p= 0.0013$, Ctrl n=16 gonads; *org1* OE n=18 gonads, Mann-Whitney Test). Scale bars, 10 um. n≥3 trials.

The accumulation of Islet in response to *org1* parallels the transcriptional cascade that specifies embryonic alary muscle specification (Boukhatmi et al., 2014). We thus hypothesized that *islet*

375 may also play a role in continued specification of niche identity in addition to the role we
376 previously found during assembly (Anllo & DiNardo, 2022). To test this hypothesis, we
377 quantified the number of Fas3 accumulating niche cells in *islet* mutants compared to controls.
378 Indeed, we counted fewer Fas3 accumulating cells in *islet* mutants, supporting our hypothesis
379 (Figure 6A-6C). This reduction in Fas3 accumulating cells is less striking than the complete loss
380 of Fas3 accumulation in the majority of *org1* mutant gonads (Figure 2A-B; 3E), suggesting a
381 more prominent role for *org1* in continued niche specification.

382 To further support a role for *islet* in niche specification downstream of *org1,* we asked whether
383 we could rescue *org1* mutant niche cell number with *islet* overexpression. We overexpressed
384 *islet* with our SGP lineage-specific driver *six4*-gal4. In gonads with both the *org1* mutation and
385 SGP-specific restoration of *islet*, we saw increased numbers of niche cells compared to *org1*
386 mutants alone (Figure 6G-6J'), supporting an ability to rescue niche cell identity. While niche cell
387 number increased with *islet* overexpression, this number was still not fully rescued to control
388 levels, and *islet* overexpression in control genetic backgrounds does not significantly increase
389 niche cell number (Figure 6G). These results suggest that while *islet* clearly contributes to niche
390 identity, its expression alone is not fully sufficient to induce niche cell fate. The partial rescue
391 also suggests that *islet* is not the only relevant *org1* target for continued specification. Taken
392 together, our results support a role for *islet* in niche cell specification and suggest that it acts
393 downstream of *org1* in this role.

394

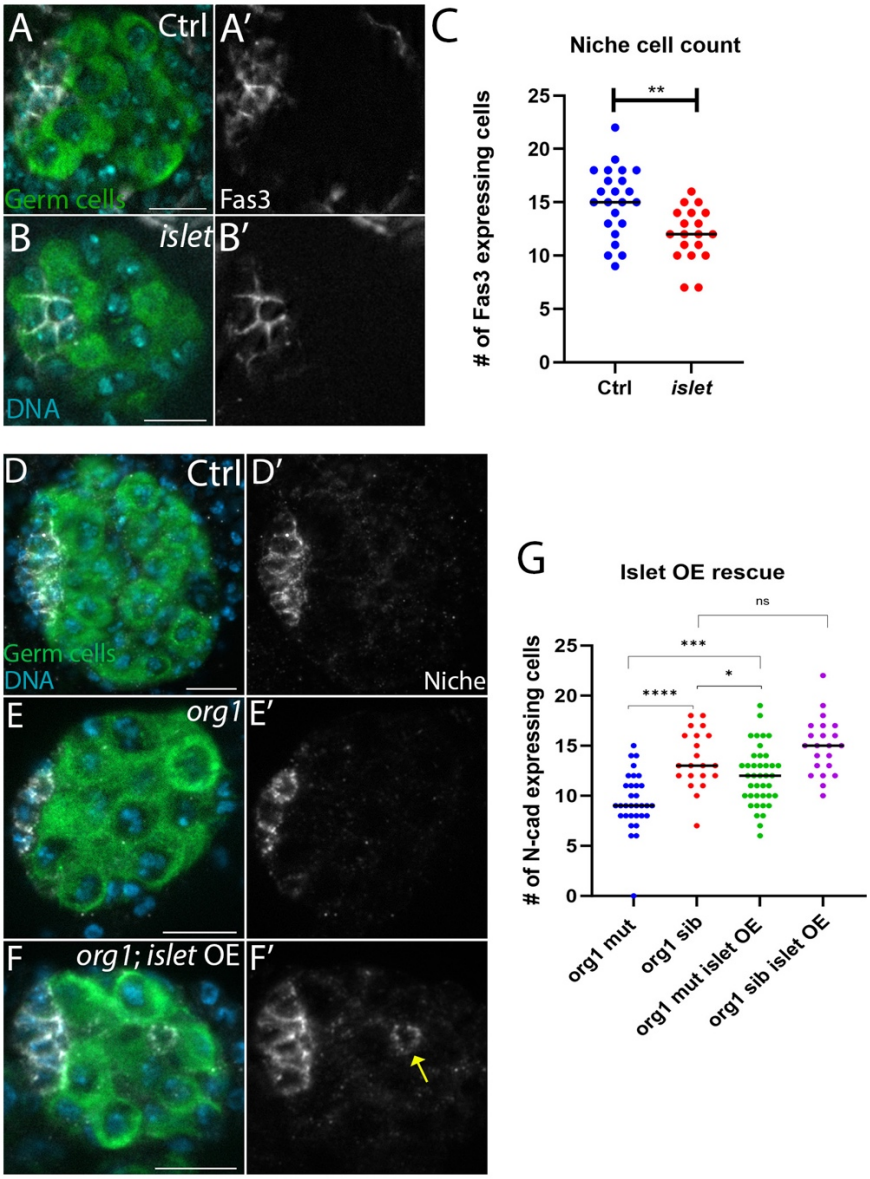

Figure 6. *islet* regulates niche cell specification downstream of *org1*. Germ cells (Vasa, green), DNA (Hoechst, blue), Niche cells (white). Scale bars, 10 um. (A, A') Control gonads with niche (Fas3, white) at the anterior. (B, B') *islet* mutant gonad with disrupted niche (Fas3, white). (C) Quantification of niche cells per gonad in *islet* mutants (p= 0.0019, Ctrl n=23 gonads; *islet* n=19 gonads, Mann-Whitney Test). (D, D') Control gonads with N-cad (white) and Islet (red) accumulating in niche cells. (E, E') *org1* mutant gonad with fewer niche cells accumulating N-cad at the anterior. (F, F') An *org1* mutant with *islet* overexpression in somatic gonadal cells had more niche cells than *org1* mutants, and a displaced niche cell (yellow arrow). (G) Number of niche cells per gonad for *org1* rescue with *islet* overexpression experiments (*org1* mut vs *org1* sib, p<0.0001, *org1* mut n=32 gonads; *org1* sib n=21 gonads. *org1* mut vs *org1* mut *islet* OE, p=0.0005, *org1* mut n=32 gonads; *org1* mut *islet* OE n=40 gonads. *org1* sib vs *org1* mut *islet* OE, p=0.0338, *org1* sib n=21 gonads; *org1* mut *islet* OE n=40 gonads. *org1* sib vs *org1* sib *islet* OE, not significant, *org1* sib n=21 gonads; *org1* sib *islet* OE n=22 gonads) Mann-Whitney Tests. Scale bars, 10 um. n≥3 trials.

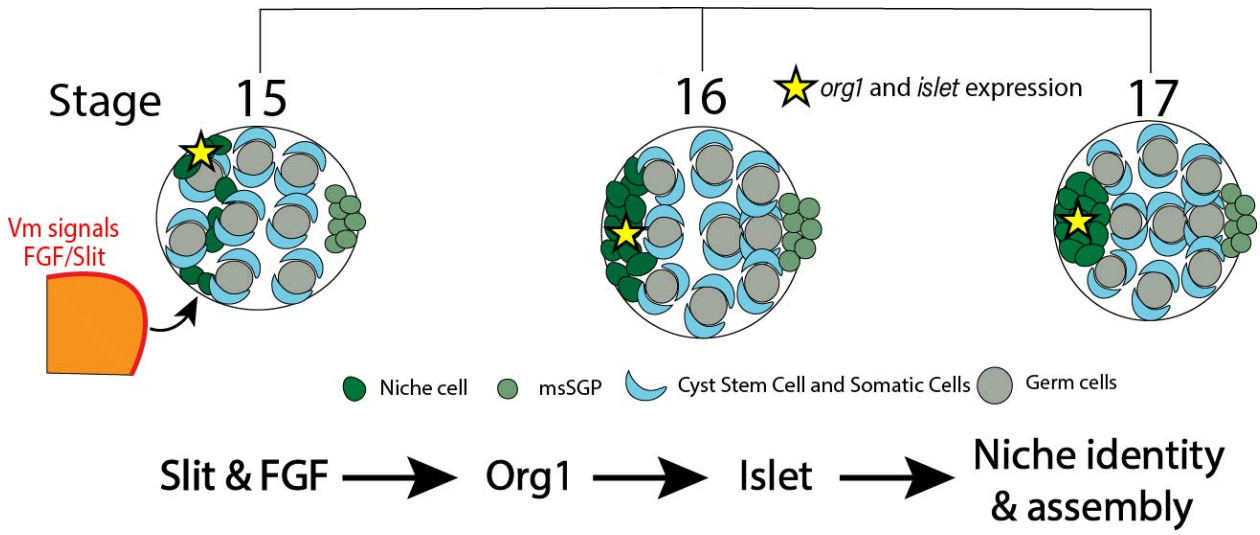

410

411 **Figure 7. Predicted model of establishment of niche identity and assembly.** Diffusible
412 signals Slit and FGF regulate *org1*. The Visceral muscle (Vm) is a neighboring tissue source of
413 both signals. *org1* functions to regulate *islet* for niche identity and assembly.
414

415 **Discussion:**

416 An impressive body of work has explored stem cell and niche functions (Anllo & DiNardo, 2022;
417 Kaestner et. al., 2019; Losick et al., 2011; Morrison & Spradling, 2008; Sato et al., 2011; Vida et
418 al., 2024; Warder et. al., 2024; Wei et al., 2023; Yamashita et al., 2005), yet how niche cells
419 acquire their identity and are positioned to properly regulate resident stem cells is largely
420 unknown. Prior to our work, Notch signaling and a downstream transcriptional regulator, *traffic*
421 *jam,* were identified as inputs to *Drosophila* testis niche identity (Kitadate & Kobayashi, 2010;
422 Okegbe & DiNardo, 2011; Wingert & DiNardo, 2015). These inputs are first induced by early
423 contact with the developing gut (Okegbe & DiNardo, 2011). Our previous work studying extrinsic
424 signals important for niche establishment has linked niche assembly with niche function in this
425 system (Anllo & DiNardo, 2022), and prior work has linked niche cell identity and assembly
426 (Wingert & DiNardo, 2015). Here, we have identified a novel regulator that further supports a
427 connection between the processes of niche identity and assembly, the Tbx1 ortholog *org1*. We
428 show that *org1* is expressed in response to Slit and FGF signals, which we previously identified
429 as niche assembly cues from neighboring visceral muscle (Anllo & DiNardo, 2022; this work). In
430 addition, we have defined *islet* as a regulator of niche identity operating downstream of *org1* (Fig
431 7, model). The combination of these factors suggests that niche assembly and identity are
432 controlled through overlapping processes. Our work addresses a knowledge gap in mechanisms
433 establishing a functional stem cell niche.

434

435 **Testis niche identity and assembly are linked**

436 Our previous work showed that the Visceral muscle signals Slit and FGF are required for niche
437 assembly. When niche assembly was compromised, niche function was also disrupted even
438 though these manipulations did not directly affect niche identity (Anllo & DiNardo, 2022).
439 Previous work suggested a connection between niche identity and assembly (Wingert &
440 DiNardo, 2015). In response to the niche specification signal Notch, the Maf transcription factor
441 *traffic jam* (*tj*) is downregulated. *traffic jam* mutants specify additional niche cells that do not
442 express all niche identity markers, and as a result do not assemble at the anterior (Wingert &
443 DiNardo, 2015). Interestingly, activating other requirements of niche identity such as Bowl
444 places the additional *tj* mutant niche cells at the gonad anterior (Wingert & DiNardo, 2015;
445 DiNardo et al., 2011). This suggests that reduction of *traffic jam* alone is not sufficient for niche
446 assembly at the anterior, supporting a role for additional regulators specifying niche cells
447 capable of assembly. Perhaps the signals necessary for anterior assembly (Slit and FGF) are
448 unable to be received by ectopic niche cells in *tj* mutants.

449

450 We have shown that niche assembly signals Slit and FGF are important for regulating the novel
451 niche identity regulator *org1*. Gonads with compromised *org1* show disruptions to markers of
452 niche identity, including complete loss of Fas3, reduction of *hh*, loss of *upd1* expression, and
453 fewer cells accumulating N-cadherin. The few niche cells that do accumulate N-cad exhibit
454 assembly defects in which a portion of these cells do not arrive at the anterior (this work). The
455 loss of continued niche specification after earlier Notch signaling might account for incomplete
456 assembly when *org1* is disrupted. *traffic jam* mutants show additional cells expressing some
457 niche identity markers, and a portion of these cells are also located in positions away from the
458 gonad anterior (Wingert & DiNardo, 2015). Together with work presented here, these data link
459 proper specification of niche identity with anterior assembly. While these data support that niche
460 identity is important for aspects of niche assembly, some niche cells still assemble anteriorly in
461 these instances when continued specification is disrupted. Perhaps differential adhesive sorting
462 enables partially specified pro-niche cells at the gonad anterior to assemble.
463

464 Interestingly, the loss of *slit* and *fgf* regulators do not completely mimic phenotypes seen in *org1*
465 mutants. For instance, *slit* and *fgf* signaling mutants are capable of accumulating Fas3, whereas
466 *org1* mutants do not. We detect residual Org1 accumulation in niche cells from *slit* and *fgf*
467 mutants (Figure 1) suggesting that additional regulators are impacting *org1* expression. We
468 suspect that while Slit and FGF both regulate *org1*, Slit and FGF signaling have a primary role in
469 facilitating niche cell anterior placement, while *org1* has a primary function in continued
470 specification of niche cell identity.
471

472 ***islet* has dual roles in niche identity and assembly downstream of *org1***

473 To further link niche identity and assembly, we present an exciting new role for the transcription
474 factor *islet* in niche specification in addition to the role we previously revealed for *islet* in niche
475 assembly. Together with our previous study, this work reveals that Slit and FGF signals induce
476 both *org1* and *islet* expression in niche cells (Anllo & DiNardo, 2022; this work). The visceral
477 muscle (Vm) is an exciting candidate source of the Slit and FGF ligands inducing *org1*, as previous
478 work revealed Vm as an important tissue supplying these signals for niche assembly (Anllo &
479 DiNardo, 2022). In addition, we show that *org1* regulates *islet* in the niche, as *org1* mutant niches
480 lack Islet, and niche cell numbers are increased by overexpressing *islet* in SGPs in an *org1* mutant
481 background. These data support the model of a transcriptional cascade regulating *islet* first
482 through Slit and FGF signals inducing *org1,* which in turn induces *islet* expression (Figure 7). *org1*

483 has a more prominent role in continued niche specification than *islet*, as *org1* mutants often lack
484 Fas3 accumulation (Figure 2A-B; 3E), whereas *islet* mutants have fewer Fas3 positive niche cells
485 (Figure 6B). This result, along with the finding that *islet* overexpression only partially rescues niche
486 cell number (Figure 6E), suggests that other genes act downstream of *org1* in addition to *islet*.
487 Interesting questions that remain include identifying these additional *org1* targets that contribute
488 to continued specification, and revealing how *islet* influences the number of niche cells that
489 accumulate Fas3 and N-cad.
490
491 The detection of dispersed, unassembled niche cells in our *six4*VP16-gal4 driven *org1* RNAi was
492 unexpected. It is reasonable to suggest earlier and stronger knockdown driving *org1* RNAi with
493 the enhanced *six4*VP16-Gal4 driver compared to that observed with *six4*-Gal4. Since we only
494 observed assembly defects under the presumed stronger conditions, we infer that *org1* has a
495 primary role in niche cell identity and a secondary role in niche assembly.
496
497
498 ***org1* regulates testis niche identity**
499
500 In alignment with Tbx1 orthologs and their conserved role in specifying mesodermal cell types,
501 we found it fitting to test if *org1* had a role in specifying the mesodermally-derived niche cells.
502 Using the niche identity markers Fasciclin3 (Fas3), *unpaired1* (*upd1),* and *hedgehog* (*hh*), we
503 saw that *org1* mutants were unable to properly accumulate these markers (Le Bras & Van
504 Doren, 2006; Okegbe & DiNardo, 2011). *hh* and its expression have been linked to niche
505 assembly downstream of Notch (Wingert & DiNardo, 2015). Using the *hh*-lacZ reporter, we
506 detected high *hh* expression in the niche, and low expression in SGPs outside the niche (Figure
507 S2). While we find that *hh* expression is not solely restricted to the niche in the embryonic gonad
508 as it is in the adult (Amoyel et. al., 2013), our ability to detect higher *hh* expression in niche cells
509 enables us to use its upregulated expression as a reliable marker for niche identity.
510
511 There are residual niche cells in *org1* mutants, which suggests that other inputs of niche identity
512 are partly active. It has been previously described that Notch signaling is necessary for
513 specifying niche cells (Kitadate & Kobayashi, 2010; Okegbe & DiNardo, 2011). The average
514 number of niche cells in Notch mutants is far fewer than we see in *org1* mutants, which
515 suggested to us that *org1* is either one of multiple effectors downstream of Notch or involved in
516 a parallel niche specification mechanism. One of the effects of Notch signaling in specifying

517 niche cells is to downregulate Traffic jam (Tj) accumulation in these cells. Previously, it was not
518 known when downregulation of *traffic jam* began in prospective niche cells (Wingert & DiNardo,
519 2015). We detected downregulation of *tj* coinciding with the beginning of *org1* expression in
520 prospective niche cells after gonad coalescence. Since *org1*-expressing cells had lowered
521 levels of Tj, we considered whether *org1* might repress Tj. However, we have shown that Tj is
522 not regulated by *org1* (Figure S2). Alternatively, Tj might block *org1* expression. This
523 relationship could explain the higher accumulation or Org1::GFP we detect in SGPs with
524 reduced Tj (Figure 1B-B'', yellow arrows). Future work should assess whether Tj regulates *org1*
525 downstream of Notch.
526
527 Our work has established *org1* as a novel regulator of identity and assembly during testis niche
528 establishment. Multiple factors identified in the *Drosophila* testis stem cell niche have translated
529 into other systems, including a role for Notch in niche specification (Zamfirescu et al., 2022).
530 Because of the numerous cell biological concepts elucidated in this niche that have translated to
531 other systems, our work lays the foundation for future studies to investigate a conserved
532 capacity of Tbx1 to specify gonadal mesoderm or niche cell fate.
533
534 **Study limitations:** While we reveal a role for *org1* in continued niche specification during
535 development, our genetic manipulations do not survive past embryogenesis. This precludes our
536 ability to assess later effects of losing *org1* during development. This work importantly reveals a
537 role for *org1* during initial niche formation, and future work will be required to study a role for
538 *org1* in adult niche maintenance. Finally, while assessing double mutant animals would be one
539 way to support evidence of *islet* downstream of *org1*, genetic odds of conducting this
540 experiment are not feasible.
541

542 **Methods:**

543 **Embryonic gonad dissection and immunostaining:**

544 Embryos were collected for 2 hours and then aged for 20-22 hours in a humidified chamber at 25
545 C to stage 17. Embryos were then sorted for mutant and control genotypes using fluorescently
546 marked balancer chromosomes (FM7DfdYFP or TM6DfdGFP). Sorted embryos were dissected
547 and immunostained as previously described (Anllo et. al. 2019). Dissected tissue was incubated
548 at 4C overnight with primary antibodies. Secondary antibodies were used at 3.75 ug/mL
549 (Alexa488, Cy3, or Alexa647; Molecular Probes; Jackson Immunoresearch) for 1.5-2 hours at
550 room temperature. DNA was stained with Hoechst33342 (Sigma) at 0.2-0.3 ug/mL for 6 minutes.
551
552 We used goat anti Vasa 1:800 (Santa Cruz Biotech -Discont.); rabbit anti Vasa 1:5000 (BosterBio
553 DZ41154); mouse anti Fasciclin III 1:50 (DSHB AB_528238); rat anti N-cadherin 1:20 (DSHB
554 AB_528121); rat anti E-cad 1:20 (DSHB AB_528120); rabbit anti Stat92E 1:200 (Flaherty et al.,
555 2010); rabbit anti RFP 1:500 (Abcam ab62341); mouse anti Islet 1:200 (DSHB AB_528313);
556 guinea pig anti Traffic jam 1:10,000 (Gift from D. Godt); rat anti Org-1 1:200 (gift from C. Schaub);
557 mouse anti Gamma Tubulin 1:200 (Sigma AB_477584); chicken anti Beta-gal 1:1000 (Abcam
558 ab9361-250); mouse anti Patched 1:50 (DSHB AB_528441); and chicken anti GFP 1:1000 (Aves
559 labs AB_2307313).
560
561 Tissue was imaging using a Zeiss AxioImager.Z1 microscope equipped with and ApoTome.2, X-
562 cite Xylis fluorescent light source, and Axiocam 705 mono camera, using 40x 1.2 N.A. plan apo
563 lens. Org1::GFP reporter images in Stage 15 embryos were obtained with a Crest X-Light V3
564 spinning disk confocal on an Olympus IX83 platform with a 60x 1.3 N.A. plan apo silicone oil
565 immersion objective.
566

567 **Visualization of Stage 15 embryonic gonads:**

568 Embryos were collected on grape juice agar plates supplemented with a dab of fresh yeast paste.
569 After allowing adult flies to lay fertilized eggs for 16 h, the embryos were transferred to a nylon
570 mesh strainer by rinsing with de-ionized water and using a paintbrush. Embryos were de-
571 chorionated with 50% bleach for no longer than 5 min. Embryos were fixed in a glass vial at 23
572 degrees C in a 1:1 mixture of 4% paraformadelhyde (PFA) in PBS:heptane for 18 min while on a
573 nutator (Mitchison and Sedat, 1983). The PFA was removed and replaced with an equal volume
574 of 100% methanol. The vial was vigorously shaken for 30-60 seconds to devitellinize the embryos.
575 Heptane was then removed, and devitellinized embryos were washed with 100% methanol three

576 times. Embryos were washed once with 50% methanol in phosphate buffered saline (PBS), then
577 again with 100% PBS with 0.1% Triton for gentle rehydration. Embryos were blocked for at least
578 1 hour in 4% Normal Donkey Serum, prior to immunostaining and imaging as described above.
579 Stage 15 embryos selected for imaging based on Campos-Ortega and Hartenstein (1985).
580
581 ***Drosophila* strains:**
582 All *Drosophila* lines used are listed in the Key Resources Table. *org1[OJ487]* is a null allele lacking
583 the translation initiation codon and T-box domain (Schaub et al., 2012). Org1::GFP is a bacterial
584 artificial chromosome (BAC) including the *org1* coding sequence and nearby genetic regulatory
585 elements upstream of an in-frame GFP sequence (Kudron et al., 2018). We have confirmed that
586 this BAC rescues *org1* lethality (data not shown). *slit[2]* is a null allele with no detectable protein
587 product (Battye et. al., 2001; Nusslein-Volhard et. al., 1984). To remove *pyr* and *ths* FGF ligands
588 together, we used a small chromosomal deficiency, Df(2R)BSC25, which completely deletes the
589 genes encoding both ligands that bind the Heartless FGF receptor (Stathopoulos et al., 2004).
590 When generating *org1[OJ487]*, *upd1*-Gal4 recombinant chromosomes, we screened for
591 homozygous lethality and the ability to drive *upd1*-Gal4, UAS-redStinger expression in larval
592 tissues.
593
594 **Identification of male gonads, and the niche:**
595 We identified male gonads by the presence of male specific SGPs at the posterior (De Falco et.
596 al., 2003) which were visualized with Vasa (BosterBio) or six4moeGFP (Sano et al., 2012).
597 Additionally, male gonads can be identified by the fact that they have more proliferative germ cells
598 and therefore have more germ cells than female gonads (Anllo et. al., 2019; Wawersik et. al.,
599 2005). Niches in stage 17 embryos were identified via immunofluorescence by niche cell specific
600 accumulation of Fasciclin 3 (DSHB AB_528238), or enrichment of N-cadherin (DSHB
601 AB_528121) or E-cadherin (DSHB AB_528120).
602
603 **Characterization of niche phenotypes:**
604 When assessing morphology and proper assembly of the niche, we characterized a niche as
605 either “assembled” or “unassembled”. “Assembled” niches show all niche cells contacting one
606 another at the gonad anterior and have clearly smoothened cell boundaries around the niche
607 periphery. “Unassembled” niches have niche cells anterior and at the gonad periphery, but with
608 irregular boundaries, and/or have dispersed niche cells that are not contacting the anterior cluster
609 of niche cells.

610

611 **Rigor and Reproducibility:**

612 All experiments were conducted at least in triplicate (n≥3 trials) with sufficiently large sample sizes
613 that previously enabled detection of significant differences (significance level of less than or equal
614 to 0.05%). Genetic controls were always used, comparing perturbed conditions to the most
615 genetically similar control background feasible.

616

617 **Quantification of niche cell count:**

618 When quantifying the number of cells that express N-cad, Fas3, or any other niche marker, we
619 use the ImageJ Cell Counter Plugin to record cells that we counted manually. A niche cell will
620 accumulate Fas3 when in contact with other niche cells and will accumulate N-cad on all
621 interfaces. Niche cells that are counted with either Fas3 or N-cad are co-labeled with a nuclear
622 marker such as Traffic jam or Hoechst, to enable clear identification of distinct cells. Dispersed
623 niche cells that accumulate Fas3 do not show polarized enrichment to specific cell interfaces.

624

625 **Quantification of normalized niche cell expression/accumulation:**

626 When quantifying accumulation of proteins and reporters of gene expression, we used ImageJ
627 software to measure mean gray value fluorescence intensity within regions of interest (ROIs). We
628 selected ROIs including a circular region within somatic cell boundaries, using either Fas3 or N-
629 cad immunofluorescence to delineate niche cell boundaries and Hoechst dye to delineate nuclei.
630 ROIs were in a single Z plane in which the relevant cell was in focus. For all experiments except
631 *upd* measurements, 3 niche cell ROIs were measured from each gonad. For *upd* measurements,
632 5 niche cell ROIs were measured per gonad. To quantify background fluorescence, an ROI was
633 selected to encompass the unlabeled region of a single germ cell within each gonad, and a
634 separate background ROI drawn from a region where no tissue was present. Background-
635 subtracted fluorescence values for each niche cell were normalized, dividing by the background-
636 subtracted value from the neighboring unlabeled germ cell for the respective gonad. Relative
637 fluorescence values for each niche cell were plotted. Mann-Whitney tests were used to evaluate
638 comparisons.

639

640 **Quantification of fluorescence at cell junctions:**

641 To quantify fluorescence intensity of F-actin between cell interfaces, we used ImageJ software to
642 measure mean gray value fluorescence intensity within regions of interested (ROIs). ROIs were
643 either niche-niche interfaces or niche-GSC interfaces. We selected 4-pixel-wide segmented line

644 ROIs between niche cells and between niche cells and GSCs. 2-4 niche-niche and niche-GSC
645 interfaces were measured in every gonad using N-cad to visualize each interface. We measured
646 the mean fluorescence intensity of our Ftractin-tdTomato blindly with N-cad as a boundary. To
647 estimate background fluorescence, a separate ROI was drawn from a region where no tissue was
648 present. Background-subtracted fluorescence values for each niche cell were normalized, divided
649 by the background-subtracted average value of all cell interfaces. Relative fluorescence values
650 for each interface were plotted. Mann-Whitney tests were used to evaluate comparisons.
651
652 **Quantification of Stat accumulation:**
653 To quantify Stat accumulation, we stained gonads with a Stat antibody (E. Bach, 1:200) and used
654 ImageJ to measure the mean gray value fluorescence intensity within regions of interest (ROIs).
655 During dissections and staining, we used the phosphatase inhibitor PhosStop (Sigma –
656 Cat#4906845001). We selected ROIs including a circular region to sample germ cells, using Vasa
657 immunofluorescence as a marker to delineate cell boundaries. Whole germ cells were measured
658 in a single Z plane in which the relevant cell was in focus. We selected ROIs by only using the
659 germ cell marker to mark sample regions to avoid biased observations towards brighter or dimmer
660 fluorescence of Stat. For each gonad, we sampled all GSCs we could clearly identify and 3-7
661 neighboring germ cells in the second tier, further from the germline stem cells. After background
662 subtraction, we measured the ratio of Stat accumulation within each GSC relative to the
663 neighboring germ cell average for that gonad. Relative Stat enrichment values were plotted for
664 each GSC. We obtained measurements on mutants for *org1* and their sibling controls, and *org1*
665 RNAi knockdowns with their sibling controls. Mann-Whitney tests were used to evaluate
666 comparisons.
667
668 **Quantification of STAT+ GSCs:**
669 To determine whether a germ cell adherent to the niche was STAT+, we first counted the number
670 of germline stem cells (GSCs) directly adjacent to N-cadherin labeled niche cells. We then
671 quantified the mean fluorescence intensity from each of these adherent germ cells as described
672 above, measuring mean STAT enrichment for each adherent germ cell in *org1* RNAi knockdowns
673 and sibling control animals. We established a threshold STAT+ fluorescent value, measured as
674 one standard deviation below the relative mean fluorescence intensity of controls. For controls,
675 the relative mean fluorescence intensity was 2.76, with a standard deviation of 0.97, therefore
676 any adherent germ cells with a mean fluorescence intensity above 1.79 were counted as STAT+
677 in both control and *org1* RNAi knockdown gonads. Data were imported into Prism v10.0 to

678 generate scatterplots where each dot represents a gonad. We plotted the number of STAT+ GSCs
679 per gonad, and separately the percentage of STAT+ GSCs per gonad for *org1* RNAi and sibling
680 control conditions. A Mann–Whitney test was used to evaluate the comparison.
681
682 **Centrosome anchoring quantification:**
683 Centrosome position was visualized with immunofluorescence against Gamma tubulin to label
684 pericentriolar material. GSCs were scored for centrosome position if they had already undergone
685 centrosome duplication, indicating that they had advanced at least to the G2 stage of the cell
686 cycle (Chen et. al., 2018). We quantified how often one of the two centrosomes was positioned
687 closer to the adjacent niche, marked by N-cad, than to other neighboring cells. GSCs with a
688 centrosome located near the niche-GSC interface were scored as appropriately aligned. GSCs
689 with both centrosomes positioned away from the niche were scored as misaligned. Significance
690 was assessed with Fisher's exact test.

691 **Key Resources Table:**

Reagent Type	Designation	Source	Identifiers
Genetic reagent (D. melanogaster)	org1[OJ487]/ FM7DfdYFP or Y	Bloomington Drosophila Stock Center	Schaub et. al., 2012; RRID: BDSC_91555
Genetic reagent (D. melanogaster)	org1 RNAi (II)	Vienna Drosophila Stock Center	v104393
Genetic reagent (D. melanogaster)	UAS-org1	Bloomington Drosophila Stock Center	Schaub et. al., 2012; RRID: BDSC_92971
Genetic reagent (D. melanogaster)	*six4*-gal4/CyoDfdYFP; Dr/Tm3,sb	Anllo et al., 2019	
Genetic reagent (D. melanogaster)	*six4*VP16-gal4/CyoDfdYFP; Dr/TM3,Sb	Warder et al., 2024	
Genetic reagent (D. melanogaster)	w[*] ; P{w+ UAS-islet} on III	Bloomington Drosophila Stock Center	RRID:BDSC_39662
Genetic reagent (D. melanogaster)	ry[506], P{ry+}hhLacZ	Bloomington Drosophila Stock Center	RRID:BDSC_5530
Genetic reagent (D. melanogaster)	P-Dsix4-eGFP::Moesin	R. Lehmann	Sano et. al., 2012
Genetic reagent (D. melanogaster)	Pbac{org-1-GFP.FPTB}VK00033/ TM6C, Sb[1]	Bloomington Drosophila Stock Center	Kudron et al., 2018

Genetic reagent (D. melanogaster)	six4>ftractin tdTomato on II	Stephen DiNardo	RRID: BDSC_58989 UAS-ftractin tdTomato
Genetic reagent (D. melanogaster)	Df(2R)BSC25 – *fgf* mutant	Bloomington Drosophila Stock Center	RRID: BDSC_6865
Genetic reagent (D. melanogaster)	*slit[2]*	Bloomington Drosophila Stock Center	RRID: BDSC_3266 (Battye et. al., 2001; Nusslein-Volhard et. al., 1984)
Genetic reagent (D. melanogaster)	tupex4	S. Campuzano	FBal0216723; (Stathopoulos et al., 2004).
Genetic reagent (D. melanogaster)	*nos*-lifeactin-tdTomato	B. Lin; R. Lehmann	(Lin et al., 2020)
Genetic reagent (D. melanogaster)	*upd1*-Gal4	Bloomington Drosophila Stock Center	RRID: BDSC_26796
Genetic reagent (D. melanogaster)	UAS-redStinger	Bloomington Drosophila Stock Center	RRID: BDSC_8547
Antibody	Goat polyclonal anti-Vasa	Santa Cruz Biotechnology	RRID:AB_793880 Discontinued
Antibody	Mouse monoclonal anti Fasciclin III	Developmental Studies Hybridoma Bank	RRID:AB_528238
Antibody	Rabbit polyclonal anti STAT92E	E. Bach	
Antibody	Rabbit polyclonal anti RFP	Abcam	RRID:AB_945213

Antibody	Mouse monoclonal anti Islet	Developmental Studies Hybridoma Bank	RRID:AB_528313
Antibody	Guinea pig polyclonal anti Traffic jam	D. Godt	
Antibody	Rat anti Org-1	C. Shaub	
Antibody	Mouse monoclonal anti Gamma-tubulin	Sigma	RRID:AB_477584
Antibody	Rabbit Polyclonal anti Vasa	Boster Bio	DZ41154
Antibody	Chicken polyclonal anti Beta-gal	Abcam	ab9361-250
Antibody	Mouse Monoclonal anti Patched	Developmental Studies Hybridoma Bank	RRID: AB_528441
Antibody	Rat monoclonal anti CadN	Developmental Studies Hybridoma Bank	RRID: AB_528121
Antibody	Rat monoclonal anti CadE	Developmental Studies Hybridoma Bank	RRID: AB_528120
Antibody	Chick polyclonal anti GFP	Aves Labs	RRID: AB_2307313
Antibody	Alexafluor Secondary Antibodies (488, 647)	Molecular Probes	
Antibody	Cy3 Affinipure Secondary Antibodies	Jackson ImmunoResearch	RRID: AB_2307443
Chemical Compound, Drug	Hoechst	Sigma	Cat#33342; CAS Number: 875756-97-1
Chemical Compound, Drug	Normal Donkey Serum (NDS)	Jackson Immunoresearch Laboratories	RRID: AB_2337258

Chemical Compound, Drug	Ringers		doi:10.1101/pdb.rec12409
Chemical Compound, Drug	Heptane		
Chemical Compound, Drug	Propyl-gallate	Sigma Aldrich	SKU: P3130; CAS Number 121-79-9
Chemical Compound, Drug	Para-Formaldehyde (PFA), 16%	Electron Microscopy Sciences	Cat#15710
Chemical Compound, Drug	Phosphatase inhibitor (PhosphaSTOP)	Roche/Sigma	Cat#4906845001
Software, Algorithm	FIJI (Image J)	www.fiji.sc	
Software, Algorithm	Image J	www.imagej.nih.gov/ij/	
Software, Algorithm	Graphpad Prism	Graphpad Software	RRID:SCR_002798
Software, Algorithm	Axio-Vision Imaging Software	Zeiss	v4.8.1
Software, Algorithm	Adobe Photoshop	https://www.adobe.com/uk/products/photoshop.html	RRID:SCR_014199
Equipment	Zeiss Axioimager.Z1	Zeiss	
Equipment	ApoTome.2	Zeiss	
Equipment	Xcite Xylis	Zeiss	
Equipment	40x 1.2 NA objective	Zeiss	
Equipment	Leica M165FC	Leica	

Equipment	GFP Filter set ET470/ 40x; ET525/50m	Leica 10447408	

692

693

694 **Supplemental Figures:**

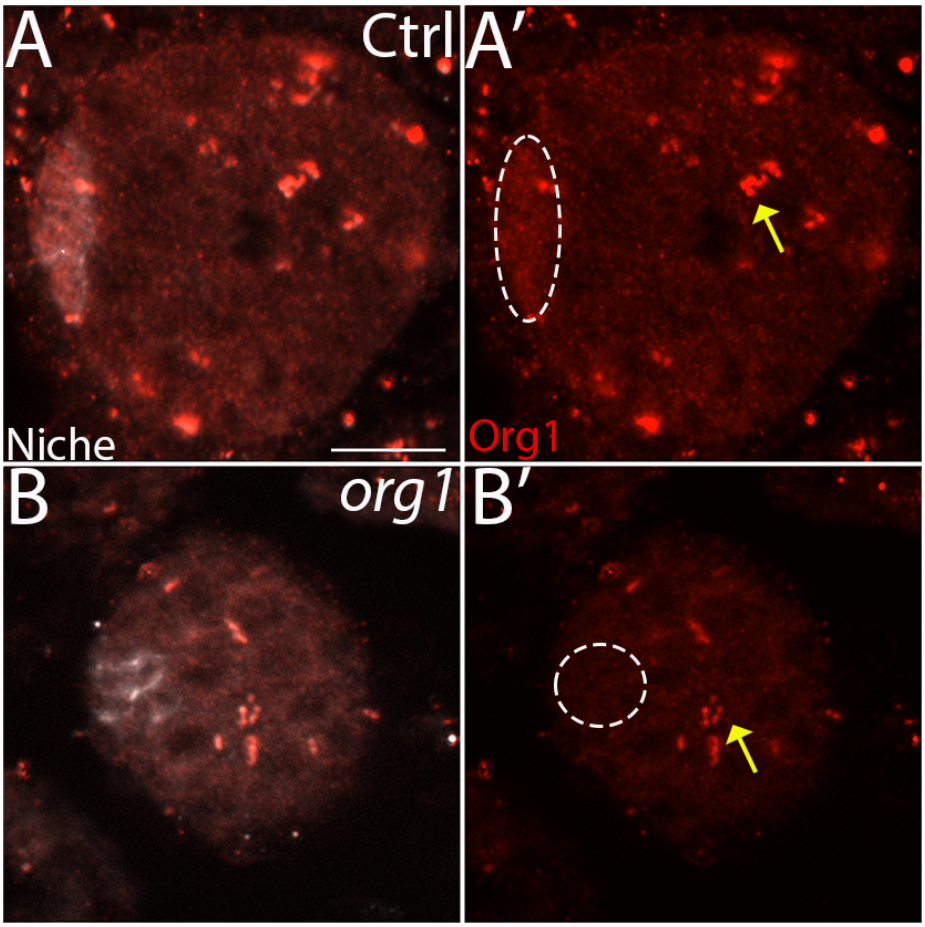

695

696 **Figure S1. Org1 antibody validation in *org1* mutants.** (A, A') Control gonads with Org1
697 accumulation (red) in the niche (Fas3, white) at the anterior, along with variable punctate signal
698 in other places in the gonad (yellow arrow). (B, B') *org1* mutant gonads with no Org1
699 accumulation (red) in the niche (white) at the anterior. Note that the variable punctate signal still
700 persists (yellow arrow) in the mutant and is thus spurious background and cannot be due to
701 Org1. Scale bars, 10 um.
702

703

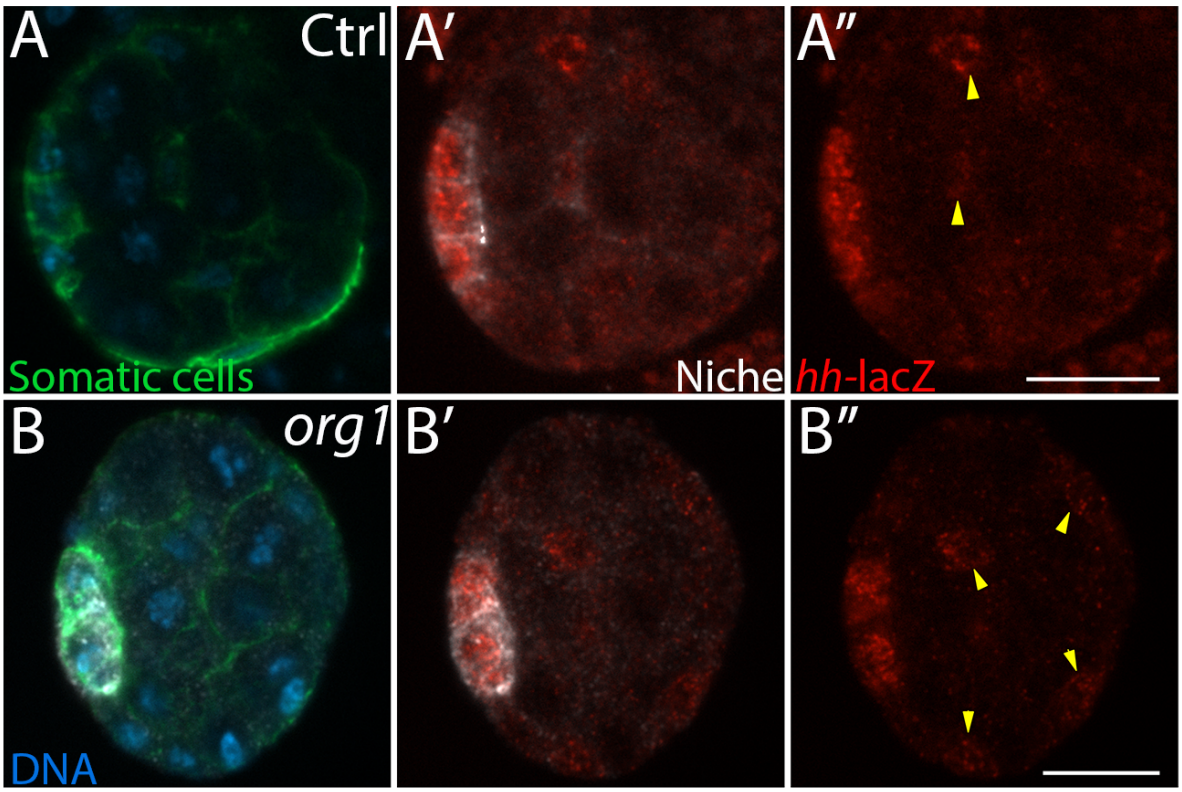

Figure S2. *hh* is expressed outside of the niche. Somatic cells (green), Niche (white), *hh*-lacZ (red), DNA (blue). (A-A”) *hh*-lacZ reporter can be seen at high levels in niche cells, with lower levels of expression outside of the niche (yellow arrows) in control gonads. (B-B”) *org1* mutant gonads with low *hh*-lacZ expression in the niche (quantification in Fig 2), and outside of the niche (yellow arrows).

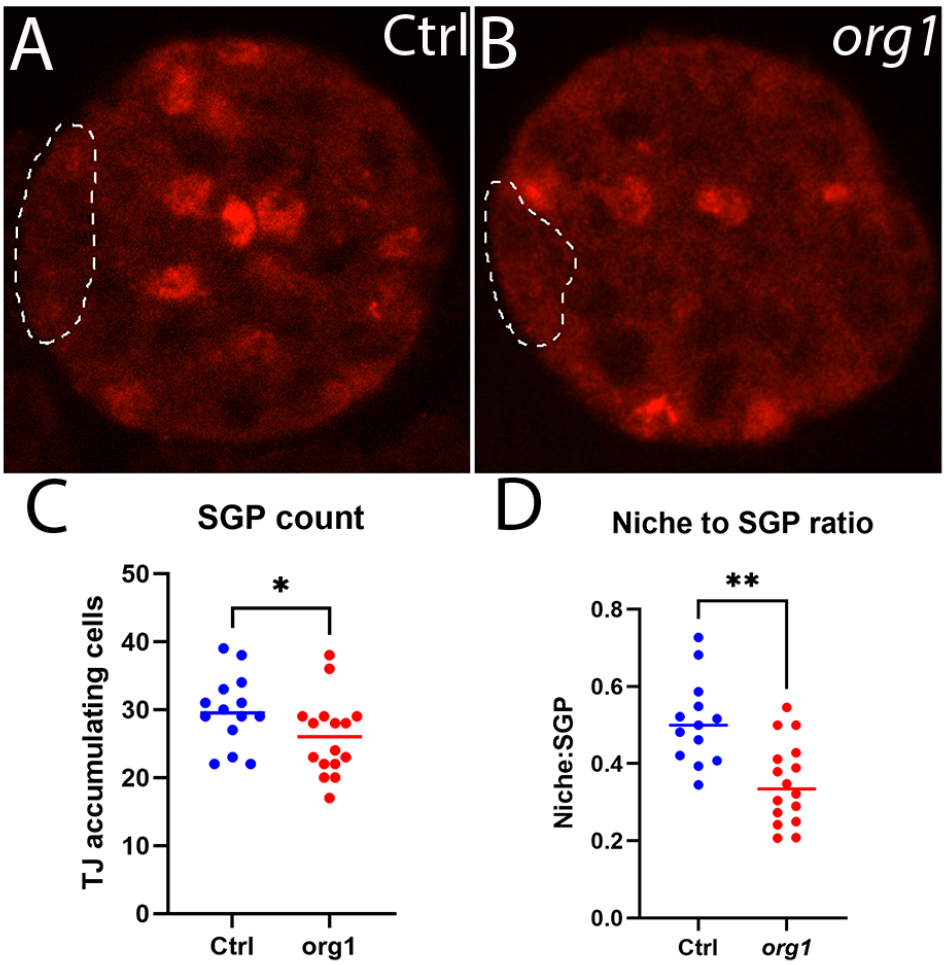

Figure S3. *org1* mutants exhibit a lower ratio of niche cells relative to number of SGPs. (A) Control and (B) *org1* mutant gonads with Traffic jam accumulation. Niches are outlined with dotted lines. (C) Quantification of number of Traffic jam accumulating SGPs indicated fewer SGPs in *org1* mutants versus controls ($p = 0.0399$, Ctrl n= 14 gonads; *org1* n=16 gonads, Mann-Whitney test). (D) Quantification of SGP to Niche cell ratio showed a lower ratio of niche cells relative to SGPs in *org1* mutants ($p = 0.0010$, Ctrl n=13 gonads; *org1* n=16 gonads, Mann-Whitney test). Scale bars, 10 um.

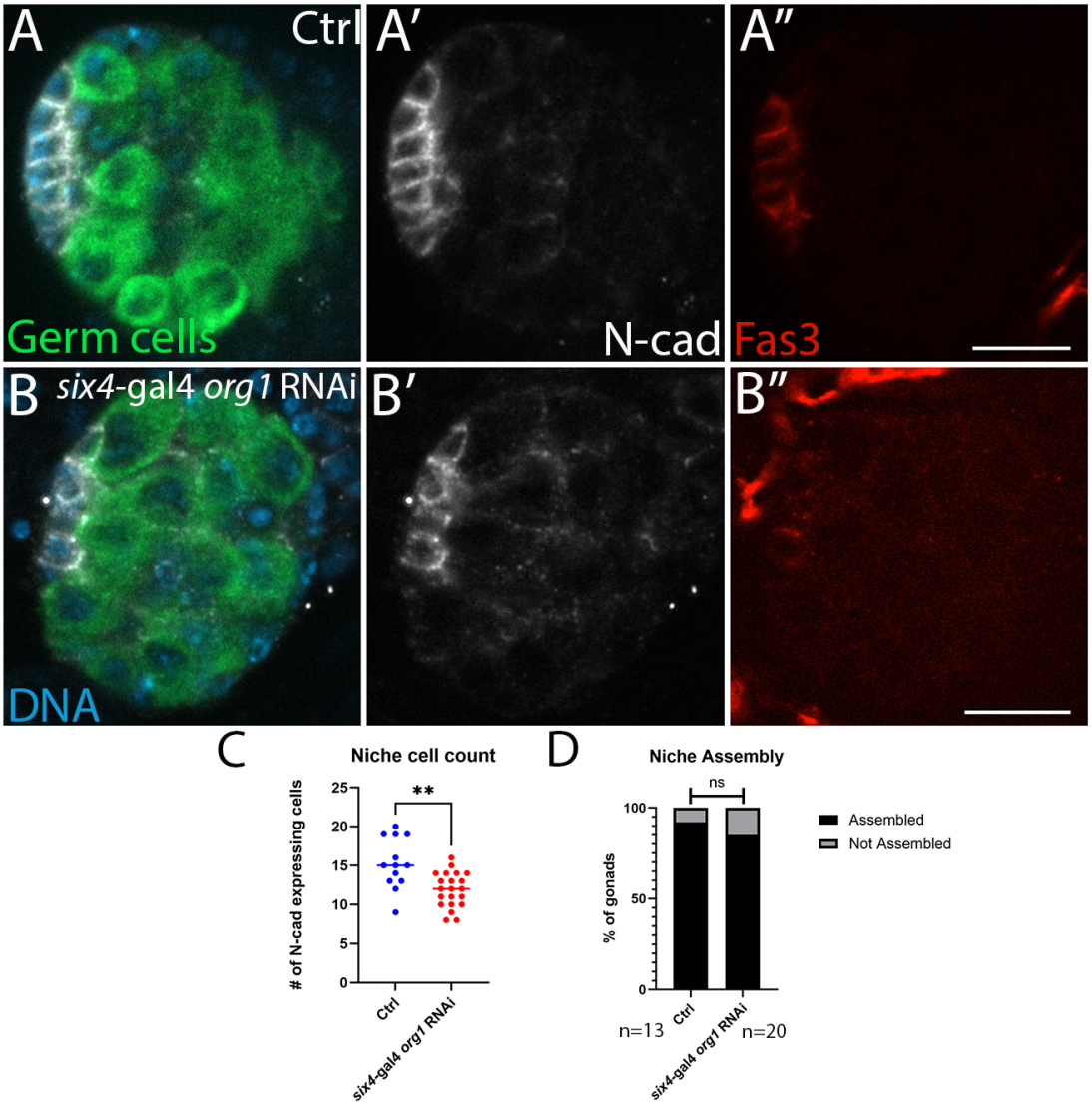

720

721 **Figure S4. *org1* RNAi with a Gal4 driver shows identity defects but not assembly defects.**
722 Germ cells (green), N-cad (white), Fas3 (red), DNA (blue). (A-A') Control gonads with
723 assembled niches and clear Fas3 accumulation. (B,B') *six4*gal4 > *org1* RNAi gonads with fewer
724 niche cells and reduced Fas3 accumulation. (C) Quantification of niche cell count in six4-gal4
725 *org1* RNAi gonads (p= 0.0022, Ctrl n=13 gonads; *six4*-gal4 *org1* RNAi n=21 gonads, Mann-
726 Whitney Test). (D) Quantification of assembly defects in six4-gal4 *org1* RNAi gonads (p> 0.99,
727 Ctrl n=13 gonads; *six4*-gal4 *org1* RNAi n=20, Mann-Whitney Test). Scale bars, 10 um.
728

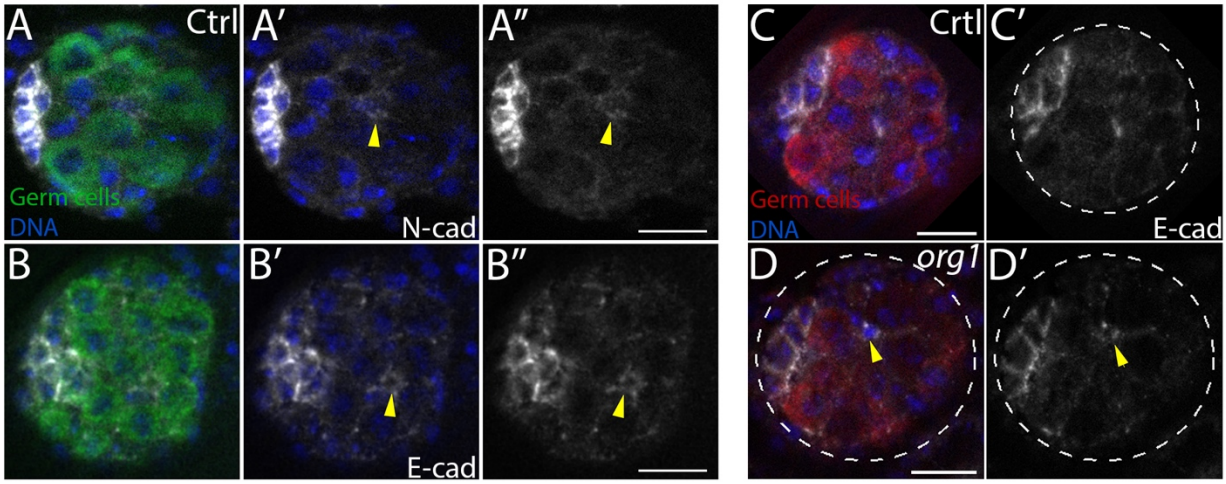

Figure S5. N-cad and E-cad can be found spuriously in SGPs outside of the niche. (A-B”) Control gonads immunostained to show germ cells (green) and DNA (blue). (A) N-cad (white) and (B) E-cad can be seen in an SGP (yellow arrow) outside of the niche but is not as enriched at the cell cortex as in the anterior niche. (C-D’) Germ cells (red), E-cad (white), DNA (blue). (C, C’) Control gonad with E-cad enriched in the cortex of niche cells. (D, D’) *org1* mutant gonad with E-cad enriched to similar levels in a presumptive lost niche cell outside of the anterior niche (yellow arrow). Scale bars, 10 um.

Table S1. Supplementary Genotype Table (next page).

Figure	Panel	Genotype	Full Genotype
1	A	*org1* reporter	org1::GFP Bac / org1::GFP Bac (on III)
1	B	*org1* reporter	org1::GFP Bac / org1::GFP Bac (on III)
1	C	*org1* reporter	org1::GFP Bac / org1::GFP Bac (on III)
1	D	Antibody	CyO, DfdGFP / +
1	E	Ctrl	CyO, DfdGFP / +
1	F	*slit, fgf*	*slit[2]*, Df(2R)BSC25 / *slit[2]*, Df(2R)BSC25
1	G	*fgf*	Df(2R)BSC25 / Df(2R)BSC25
1	H	*slit*	*slit[2] / slit[2]*
1	I	Ctrl	CyO, DfdGFP / +
1	I	*slit, fgf*	*slit[2]*, Df(2R)BSC25 / *slit[2]*, Df(2R)BSC25
1	J	het	Df(2R)BSC25 / CyO, DfdGFP
1	J	mut	Df(2R)BSC25 / Df(2R)BSC25
1	K	het	slit[2] / CyO, DfdYFP
1	K	mut	*slit[2] / slit[2]*
2	A	Ctrl	FM7, DfdGfP / Y
2	B	*org1*	*org1[OJ487]* / Y
2	C	Ctrl	FM7, DfdGfP / Y ; *six4* moesinGFP / + ; hh-LacZ / +
2	D	*org1*	*org1[OJ487]* / Y ; *six4* moesinGFP / + ; hh-LacZ / +
2	E	Ctrl	FM7, DfdGfP / Y ; *six4* moesinGFP / + ; hh-LacZ / +
2	E	*org1*	*org1[OJ487]* / Y ; *six4* moesinGFP / + ; hh-LacZ / +
2	F	Ctrl	FM7, DfdGfP / Y
2	G	*org1*	*org1[OJ487]* / Y
2	H	Ctrl	FM7, DfdGfP / Y
2	H	*org1*	*org1[OJ487]* / Y
2	I	Ctrl	Y / + ; six4moeGFP / UAS-*org1* ; TM6, DfdGFP / UAS-*org1*
2	J	*org1* OE	Y / + ; six4moeGFP / UAS-org1; six4-gal4 / UAS-org1
2	K	Ctrl	Y / + ; six4moeGFP / UAS-*org1* ; TM6, DfdGFP / UAS-*org1*
2	K	*org1* OE	Y / + ; six4moeGFP / UAS-org1; six4-gal4 / UAS-org1
3	A	Ctrl	either *six4* VP16-Gal4 / CyO DfdGFP, or UAS-*org1* RNAi / CyO DfdGFP
3	B	*six4* VP16-Gal4 *org1* RNAi	*six4* VP16-Gal4 / UAS-*org1* RNAi
3	C	Ctrl	either *six4* VP16-Gal4 / CyO DfdGFP, or UAS-*org1* RNAi / CyO DfdGFP
3	C	*six4* VP16-Gal4 *org1* RNAi	*six4* VP16-Gal4 / UAS-*org1* RNAi
3	D	Ctrl	either *six4* VP16-Gal4 / CyO DfdGFP, or UAS-*org1* RNAi / CyO DfdGFP
3	D	*six4* VP16-Gal4 *org1* RNAi	*six4* VP16-Gal4 / UAS-*org1* RNAi
3	E	*org1*	*org1[OJ487]* / Y ; *six4*-Gal4, UAS-ftractin-TdTomato
3	E	*org1* ; *org1* OE	*org1[OJ487]* / Y ; *six4*-Gal4, UAS-ftractin-tdTomato / UAS-*org1* ; UAS-*org1* / +
3	F	Ctrl	FM7, DfdGFP / Y ; *six4*-Gal4, UAS-ftractin-TdTomato
3	G	*org1*	*org1[OJ487]* / Y ; *six4*-Gal4, UAS-ftractin-TdTomato
3	H	*org1* ; *org1* OE	*org1[OJ487]* / Y ; *six4*-Gal4, UAS-ftractin-tdTomato / UAS-*org1* ; UAS-*org1* / +
3	I	Ctrl	FM7, DfdGFP / Y ; *six4*-Gal4, UAS-ftractin-TdTomato
3	J	*org1*	*org1[OJ487]* / Y ; *six4*-Gal4, UAS-ftractin-TdTomato
3	K	*org1* ; *org1* OE	*org1[OJ487]* / Y ; *six4*-Gal4, UAS-ftractin-tdTomato / UAS-*org1* ; UAS-*org1* / +
4	A	*upd*-Gal4 with UAS-RedStinger	*upd*-Gal4 / Y ; *six4* moesinGFP / + ; UAS-redStinger / +
4	B	*upd*-Gal4, *org1* with UAS-RedStinger	*upd*-Gal4, *org1[OJ487]* / Y ; *six4* moesinGFP / + ; UAS-redStinger / +
4	C	*upd*-Gal4 with UAS-RedStinger	*upd*-Gal4 / Y ; *six4* moesinGFP / + ; UAS-redStinger / +
4	C	*upd*-Gal4, *org1* with UAS-RedStinger	*upd*-Gal4, *org1[OJ487]* / Y ; *six4* moesinGFP / + ; UAS-redStinger / +
4	D	Ctrl	FM7, DfdGfP / Y
4	E	*org1*	*org1[OJ487]* / Y
4	F	Ctrl	FM7, DfdGfP / Y
4	F	*org1*	*org1[OJ487]* / Y
4	G	Ctrl	FM7, DfdGfP / Y
4	H	*org1*	*org1[OJ487]* / Y
4	I	Ctrl	FM7, DfdGfP / Y
4	I	*org1*	*org1[OJ487]* / Y
4	J	Ctrl	FM7, DfdGfP / Y
4	K	*org1*	*org1[OJ487]* / Y
4	L	Ctrl	FM7, DfdGfP / Y
4	L	*org1*	*org1[OJ487]* / Y
4	M	Ctrl	either *six4* VP16-Gal4 / CyO DfdGFP, or UAS-*org1* RNAi / CyO DfdGFP ; *nos*-lifeactinTdTomato / +
4	N	*six4* VP16-Gal4 *org1* RNAi	*six4* VP16-Gal4 / UAS-*org1* RNAi; nos-lifeactinTdTomato / +
4	O	Ctrl	either *six4* VP16-Gal4 / CyO DfdGFP, or UAS-*org1* RNAi / CyO DfdGFP ; *nos*-lifeactinTdTomato / +
4	O	*six4* VP16-Gal4 *org1* RNAi	*six4* VP16-Gal4 / UAS-*org1* RNAi; nos-lifeactinTdTomato / +
4	P	Ctrl	either *six4* VP16-Gal4 / CyO DfdGFP, or UAS-*org1* RNAi / CyO DfdGFP
4	Q	*six4* VP16-Gal4 *org1* RNAi	*six4* VP16-Gal4 / UAS-*org1* RNAi
4	R	Ctrl	either *six4* VP16-Gal4 / CyO DfdGFP, or UAS-*org1* RNAi / CyO DfdGFP
4	R	*six4* VP16-Gal4 *org1* RNAi	*six4* VP16-Gal4 / UAS-*org1* RNAi
4	S	Ctrl	either *six4* VP16-Gal4 / CyO DfdGFP, or UAS-*org1* RNAi / CyO DfdGFP
4	S	*six4* VP16-Gal4 *org1* RNAi	*six4* VP16-Gal4 / UAS-*org1* RNAi
4	T	Ctrl	either *six4* VP16-Gal4 / CyO DfdGFP, or UAS-*org1* RNAi / CyO DfdGFP
4	T	*six4* VP16-Gal4 *org1* RNAi	*six4* VP16-Gal4 / UAS-*org1* RNAi
4	U	Ctrl	either *six4* VP16-Gal4 / CyO DfdGFP, or UAS-*org1* RNAi / CyO DfdGFP
4	U	*six4* VP16-Gal4 *org1* RNAi	*six4* VP16-Gal4 / UAS-*org1* RNAi
5	A	Ctrl	FM7, DfdGfP / Y
5	B	*org1*	*org1[OJ487]* / Y
5	C	Ctrl	FM7, DfdGfP / Y
5	C	*org1*	*org1[OJ487]* / Y
5	D	Ctrl	Y / + ; six4moeGFP / UAS-*org1* ; TM6, DfdGFP / UAS-*org1*
5	E	*org1* OE	Y / + ; six4moeGFP / UAS-org1; six4-gal4 / UAS-org1
5	F	Ctrl	Y / + ; six4moeGFP / UAS-*org1* ; TM6, DfdGFP / UAS-*org1*
5	F	*org1* OE	Y / + ; six4moeGFP / UAS-org1; six4-gal4 / UAS-org1
6	A	Ctrl	*islet[EX4]* / CyO DfdGFP
6	B	*islet*	*islet[EX4] / islet[EX4]*
6	C	Ctrl	*islet[EX4]* / CyO DfdGFP
6	C	*islet*	*islet[EX4] / islet[EX4]*
6	D	Ctrl	FM7, DfdYFP / Y ; UAS-islet / +
6	E	*org1*	*org1[OJ487]* / Y ; UAS-islet / +
6	F	*org1* ; *islet* OE	*org1[OJ487]* / Y ; UAS-islet / *six4*-Gal4
6	G	*org1* mut	*org1[OJ487]* / Y ; UAS-islet / +
6	G	*org1* sib	FM7, DfdYFP / Y ; UAS-islet / +
6	G	*org1* mut *islet* OE	*org1[OJ487]* / Y ; UAS-islet / *six4*-Gal4
6	G	*org1* sib *islet* OE	FM7, DfdYFP / Y ; UAS-islet / *six4*-Gal4
S1	A	Ctrl	FM7, DfdGfP / Y
S1	B	*org1*	*org1[OJ487]* / Y
S2	A	Ctrl	FM7, DfdGfP / Y ; *six4* moesinGFP / + ; hh-LacZ / +
S2	B	*org1*	*org1[OJ487]* / Y ; *six4* moesinGFP / + ; hh-LacZ / +
S3	A	Ctrl	FM7, DfdGfP / Y
S3	B	*org1*	*org1[OJ487]* / Y
S3	C	Ctrl	FM7, DfdGfP / Y
S3	C	*org1*	*org1[OJ487]* / Y
S3	D	Ctrl	FM7, DfdGfP / Y
S3	D	*org1*	*org1[OJ487]* / Y
S4	A	Ctrl	*six4*-Gal4 / CyO, DfdGFP
S4	B	*six4*- gal4 *org1* RNAi	*six4*-Gal4 / UAS-*org1* RNAi
S4	C	Ctrl	*six4*-Gal4 / CyO, DfdGFP
S4	C	*six4*- gal4 *org1* RNAi	*six4*-Gal4 / UAS-*org1* RNAi
S4	D	Ctrl	*six4*-Gal4 / CyO, DfdGFP
S4	D	*six4*- gal4 *org1* RNAi	*six4*-Gal4 / UAS-*org1* RNAi
S5	A	Ctrl	FM7, DfdGfP / Y
S5	B	Ctrl	FM7, DfdGfP / Y
S5	C	Ctrl	FM7, DfdGfP / Y
S5	D	*org1*	*org1[OJ487]* / Y

Acknowledgements:

We acknowledge Kirklan Naumuk for technical assistance. We thank Drs. Elizabeth Ables and Beth Thompson, and the Lenhart lab for valuable feedback on the manuscript. We thank the Bloomington *Drosophila* Stock Center (NIH P40OD018537) for stocks, and D. Godt, E. Bach and C. Schaub for antibodies.

Funding: Work was supported by NIH grants R15 GM154246 to L.A. and R35 GM136270 to S.D.

Authors have no competing interests to declare.

Author Contributions:

Conceptualization, P.H. and L.A.; methodology, L.A.; validation, P.H. & L.A.; formal analysis, P.H., A.H., T.G., and L.A.; investigation P.H., T.G., and L.A.; resources S.D. and L.A.; data curation P.H. and L.A.; writing – original draft P.H.; writing – review & editing P.H., A.H., S.D., and L.A.; visualization P.H., A.H., and L.A.; supervision S.D. and L.A.; project administration S.D. and L.A.; funding acquisition S.D. and L.A.

759 **References**

760 1. Amoyel, M., Sanny, J., Burel, M. and Bach, E. A. (2013). Hedgehog is required for CySC
761 self-renewal but does not contribute to the GSC niche in the Drosophila testis.
762 *Development (Cambridge)* 140, 56–65.
763 2. Anllo, L. and DiNardo, S. (2022). Visceral mesoderm signaling regulates assembly
764 position and function of the Drosophila testis niche. *Dev Cell* 57, 1009-1023.e5.
765 3. Anllo, L., Plasschaert, L. W., Sui, J. and DiNardo, S. (2019). Live imaging reveals hub
766 cell assembly and compaction dynamics during morphogenesis of the Drosophila testis
767 niche. *Dev Biol* 446, 102–118.
768 4. Battye, R., Stevens, A., Perry, R. L. and Jacobs, J. R. (2001). Repellent Signaling by Slit
769 Requires the Leucine-Rich Repeats.
770 5. Boukhatmi, H., Schaub, C., Bataillé, L., Reim, I., Frendo, J. L., Frasch, M. and Vincent,
771 A. (2014). An Org-1–Tup transcriptional cascade reveals different types of alary muscles
772 connecting internal organs in Drosophila. *Development (Cambridge)* 141, 3761–3771.
773 6. Boyle, M. and DiNardo, S. (1995). Specification, migration and assembly of the somatic
774 cells of the Drosophila gonad. *Development*.
775 7. Boyle, M., Bonini, N. and DiNardo, S. (1997). Expression and function of cliftin the
776 development of somatic gonadal precursors within the Drosophila mesoderm.
777 *Development*.
778 8. Campos-Ortega, J. A. and Hartenstein, V. (1985). The embryonic development of
779 *Drosophila melanogaster*. Springer-Verlag, Berlin.
780 9. Chen, C., Cummings, R., Mordovanakis, A., Hunt, A., Mayer, M., Sept, D. and
781 Yamashita, Y. (2018). Cytokine receptor-Eb1 interaction couples cell polarity and fate
782 during asymmetric cell division.
783 10. de Cuevas, M. and Matunis, E. L. (2011). The stem cell niche: Lessons from the
784 Drosophila testis. *Development* 138, 2861–2869.
785 11. DeFalco, T. J., Verney, G., Jenkins, A. B., McCaffery, J. M., Russell, S. and Van Doren,
786 M. (2003). Sex-specific apoptosis regulates sexual dimorphism in the Drosophila
787 embryonic gonad. *Dev Cell* 5, 205–216.
788 12. DiNardo, S., Okegbe, T., Wingert, L., Freilich, S. and Terry, N. (2011). Lines and bowl
789 affect the specification of cyst stem cells and niche cells in the Drosophila testis.
790 *Development* 138, 1687–1696.
791 13. Flaherty, M. S., Salis, P., Evans, C. J., Ekas, L. A., Marouf, A., Zavadil, J., Banerjee, U.
792 and Bach, E. A. (2010) *chinmo* is a functional effector of the JAK/STAT pathway that

793 regulates eye development, tumor formation, and stem cell self-renewall in *Drosophila*.
794 *Dev Cell* 18, 556-568.
795 14. Herrera, S. C. and Bach, E. A. (2019). JAK/STAT signaling in stem cells and
796 regeneration: From drosophila to vertebrates. *Development (Cambridge)* 146,.
797 15. Herrera, S. C., Sainz de la Maza, D., Grmai, L., Margolis, S., Plessel, R., Burel, M.,
798 O'Connor, M., Amoyel, M. and Bach, E. A. (2021). Proliferative stem cells maintain
799 quiescence of their niche by secreting the Activin inhibitor Follistatin. *Dev Cell* 56, 2284-
800 2294.e6.
801 16. Inaba, M., Buszczak, M. and Yamashita, Y. M. (2015). Nanotubes mediate niche-stem-
802 cell signalling in the Drosophila testis. *Nature* 523, 329–332.
803 17. Jenkins, A. B., McCaffery, J. M. and Van Doren, M. (2003). Drosophila E-cadherin is
804 essential for proper germ cell-soma interaction during gonad morphogenesis.
805 *Development* 130, 4417–4426.
806 18. Kaestner, K. H. (2019). The Intestinal Stem Cell Niche: A Central Role for Foxl1-
807 Expressing Subepithelial Telocytes. *CMGH* 8, 111–117.
808 19. Kawase, E., Wong, M. D., Ding, B. C. and Xie, T. (2004). Gbb/Bmp signaling is essential
809 for maintaining germline stem cells and for repressing bam transcription in the
810 Drosophila testis. *Development* 131, 1365–1375.
811 20. Kiger, A. A., Jones, D. L., Schulz, C., Rogers, M. and Fuller, M. (2001). Stem Cell Self-
812 Renewal Specified byJAK-STAT Activation in Response to a Support Cell Cue. *Science*
813 *(1979)* 294, 2539–2542.
814 21. Kitadate, Y. and Kobayashi, S. (2010). Notch and Egfr signaling act antagonistically to
815 regulate germ-line stem cell niche formation in Drosophila male embryonic gonads. *Proc*
816 *Natl Acad Sci U S A* 107, 14241–14246.
817 22. Kudron, M. M., Victorsen, A., Gevirtzman, L., Hillier, L. W., Fisher, W. W., Vafeados, D.,
818 Kirkey, M., Hammonds, A. S., Gersch, J., Ammouri, H., et al. (2018). The modern
819 resource: genome-wide binding profiles for hundreds of Drosophila and Caenorhabditis
820 elegans transcription factors. *Genetics* 208, 937–949.
821 23. Le Bras, S. and Van Doren, M. (2006). Development of the male germline stem cell
822 niche in Drosophila. *Dev Biol* 294, 92–103.
823 24. Leatherman, J. L. and Di Nardo, S. (2008a). Zfh-1 controls somatic stem cell self-
824 renewal in the Drosophila testis and nonautonomously influences germline stem cell
825 self-renewal. *Cell Stem Cell* 3, 44–54.

826 25. Leatherman, J. L. and Di Nardo, S. (2008b). Zfh-1 controls somatic stem cell self-
827 renewal in the Drosophila testis and nonautonomously influences germline stem cell
828 self-renewal. *Cell Stem Cell* 3, 44–54.
829 26. Leatherman, J. L. and Dinardo, S. (2010). Germline self-renewal requires cyst stem cells
830 and stat regulates niche adhesion in Drosophila testes. *Nat Cell Biol* 12, 806–811.
831 27. Lee, S., Zhou, L., Kim, J., Kalbfleisch, S. and Schöck, F. (2008). Lasp anchors the
832 Drosophila male stem cell niche and mediates spermatid individualization. *Mech Dev*
833 125, 768–776.
834 28. Lenhart, K. F. and DiNardo, S. (2015). Somatic Cell Encystment Promotes Abscission in
835 Germline Stem Cells following a Regulated Block in Cytokinesis. *Dev Cell* 34, 192–205.
836 29. Li, L. and Xie, T. (2005). Stem cell niche: Structure and function. *Annu Rev Cell Dev Biol*
837 21, 605–631.
838 30. Li, H., Janssens, J., de Waegeneer, M., Kolluru, S. S., Davie, K., Gardeux, V., Saelens,
839 W., David, F. P. A., Brbić, M., Spanier, K., et al. (2022). Fly Cell Atlas: A single-nucleus
840 transcriptomic atlas of the adult fruit fly. *Science (1979)* 375,.
841 31. Li, G., Li, Z., Li, L., Liu, S., Wu, P., Zhou, M., Li, C., Li, X., Luo, G. and Zhang, J. (2023).
842 Stem Cell-Niche Engineering via Multifunctional Hydrogel Potentiates Stem Cell
843 Therapies for Inflammatory Bone Loss. *Adv Funct Mater* 33,.
844 32. Lin, B., Luo, J., and Lehmann, R. (2020). Collectively stabilizing and orienting posterior
845 migratory forces disperses cell clusters in vivo. *Nature Communications* 11, 4477.
846 33. Losick, V. P., Morris, L. X., Fox, D. T. and Spradling, A. (2011). Drosophila Stem Cell
847 Niches: A Decade of Discovery Suggests a Unified View of Stem Cell Regulation. *Dev*
848 *Cell* 21, 159–171.
849 34. Marcellini, S., Technau, U., Smith, J. C. and Lemaire, P. (2003). Evolution of Brachyury
850 proteins: Identification of a novel regulatory domain conserved within Bilateria. *Dev Biol*
851 260, 352–361.
852 35. Michel, M., Kupinski, A. P., Raabe, I. and Bökel, C. (2012). Hh signalling is essential for
853 somatic stem cell maintenance in the drosophila testis niche. *J Cell Sci* 125, 2663–2669.
854 36. Mitchison, T.J. and Sedat, J. (1983). Localization of antigenic determinants in whole
855 *Drosophila* embryos. *Dev Biol* 99, 261-264.
856 37. Morrison, S. J. and Spradling, A. C. (2008). Stem Cells and Niches: Mechanisms That
857 Promote Stem Cell Maintenance throughout Life. *Cell* 132, 598–611.

858 38. Nusslein-Volhard, C., Wieschaus, E. and Kluding, H. (1984). Roux's Archives of
859 Developmental Biology Mutations affecting the pattern of the larval cuticle in Drosophila
860 melanogaster I. Zygotic loci on the second chromosome.
861 39. Okegbe, T. C. and di Nardo, S. (2011). The endoderm specifies the mesodermal niche
862 for the germline in Drosophila via Delta-Notch signaling. *Development* 138, 1259–1267.
863 40. Riechmann, V., Rehorn, K.-P., Reuter, R. and Leptin, M. (1998). The genetic control of
864 the distinction between fat body and gonadal mesoderm in Drosophila. *Development*.
865 41. Roach, T. V. and Lenhart, K. F. (2024). Mating-induced Ecdysone in the testis disrupts
866 soma-germline contacts and stem cell cytokinesis. *Development (Cambridge)* 151,.
867 42. Sato, T., Van Es, J. H., Snippert, H. J., Stange, D. E., Vries, R. G., Van Den Born, M.,
868 Barker, N., Shroyer, N. F., Van De Wetering, M. and Clevers, H. (2011). Paneth cells
869 constitute the niche for Lgr5 stem cells in intestinal crypts. *Nature* 469, 415–418.
870 43. Schaub, C., Nagaso, H., Jin, H. and Frasch, M. (2012). Org-1, the Drosophila ortholog of
871 Tbx1, is a direct activator of known identity genes during muscle specification.
872 *Development* 139, 1001–1012.
873 44. Sheng, X. R., Posenau, T., Gumulak-Smith, J. J., Matunis, E., Van Doren, M. and
874 Wawersik, M. (2009). Jak-STAT regulation of male germline stem cell establishment
875 during Drosophila embryogenesis. *Dev Biol* 334, 335–344.
876 45. Sinden, D., Badgett, M., Fry, J., Jones, T., Palmen, R., Sheng, X., Simmons, A., Matunis,
877 E. and Wawersik, M. (2012). Jak-STAT regulation of cyst stem cell development in the
878 Drosophila testis. *Dev Biol* 372, 5–16.
879 46. Stathopoulos, A., Tam, B., Ronshaugen, M., Frasch, M. and Levine, M. (2004). Pyramus
880 and thisbe: FGF genes that pattern the mesoderm of Drosophila embryos. *Genes Dev*
881 18, 687–699.
882 47. Tanentzapf, G., Devenport, D., Godt, D. and Brown, N. H. (2007). Integrin-dependent
883 anchoring of a stem-cell niche. *Nat Cell Biol* 9, 1413–1418.
884 48. Tseng, C. Y., Burel, M., Cammer, M., Harsh, S., Flaherty, M. S., Baumgartner, S. and
885 Bach, E. A. (2022). chinmo-mutant spermatogonial stem cells cause mitotic drive by
886 evicting non-mutant neighbors from the niche. *Dev Cell* 57, 80-94.e7.
887 49. Tulina, N. and Matunis, E. (2001). Control of Stem Cell Self-Renewal in Drosophila
888 Spermatogenesis by JAK-STAT Signaling. *Science (1979)* 294, 2546–2548.
889 50. Vida, G. S., Botto, E. and Dinardo, S. (2024). *Maintenance of niche architecture requires*
890 *actomyosin and enables proper stem cell signaling and oriented division in the*
891 *Drosophila testis*.

892 51. Walker, M. R., Patel, K. K. and Stappenbeck, T. S. (2008). The stem cell niche. *Journal*
893 *of Pathology* 217, 169–180.
894 52. Warder, B. N., Nelson, K. A., Sui, J., Anllo, L. and DiNardo, S. (2024). An actomyosin
895 network organizes niche morphology and responds to feedback from recruited stem
896 cells.
897 53. Wawersik, M., Milutinovich, A., Casper, A. L., Matunis, E., Williams, B. and Van Doren,
898 M. (2005). Somatic control of germline sexual development is mediated by the
899 JAK/STAT pathway. *Nature* 436, 563–567.
900 54. Wingert, L. and DiNardo, S. (2015). Traffic jam functions in a branched pathway from
901 Notch activation to niche cell fate. *Development (Cambridge)* 142, 2268–2277.
902 55. Yamashita, Y., Jones, L. and Fuller, M. (2003). Orientation of Asymmetric StemCell
903 Division by the APC TumorSuppressor and Centrosome. *Science (1979)* 301, 1547–
904 1550.
905 56. Yamashita, Y. M., Fuller, M. T. and Jones, D. L. (2005). Signaling in stem cell niches:
906 Lessons from the Drosophila germline. *J Cell Sci* 118, 665–672.
907 57. Zamfirescu, A-M., Yatsenko, AS., and Shcherbata, HR. (2022). Notch signaling sculpts
908 the stem cell niche. Front. Cell Dev. Biol. 10:1027222
909 **58.** Zheng, Q., Wang, Y., Vargas, E. and DiNardo, S. (2011). Magu is required for germline
910 stem cell self-renewal through BMP signaling in the Drosophila testis. *Dev Biol* 357,
911 202–210